

GRAPH LAPLACIAN ASSISTED REGULARIZATION METHOD UNDER NOISE LEVEL FREE HEURISTIC AND STATISTICAL STOPPING RULE

HARSHIT BAJPAI AND ANKIK KUMAR GIRI

Abstract. In this work, we address the solution of both linear and nonlinear ill-posed inverse problems by developing a novel graph-based regularization framework, where the regularization term is formulated through an iteratively updated graph Laplacian. The proposed approach operates without prior knowledge of the noise level and employs two distinct stopping criteria namely, the heuristic rule and the statistical discrepancy principle. To facilitate the latter, we utilize averaged measurements derived from multiple repeated observations. We provide a detailed convergence analysis of the method in statistical prospective, establishing its stability and regularization properties under both stopping strategies. The algorithm begins with the computation of an initial reconstruction using any suitable techniques like Tikhonov regularization (Tik), filtered back projection (FBP) or total variation (TV), which is used as the foundation for generating the initial graph Laplacian. The reconstruction is made better step by step using an iterative process, during which the graph Laplacian is dynamically re-calibrated to reflect how the solution's structure is changing. Finally, we present numerical experiments on X-ray Computed Tomography (CT) and phase retrieval CT, demonstrating the effectiveness and robustness of the proposed method and comparing its reconstruction performance under both stopping rules.

Keywords: data-assisted regularization, unknown noise level, statistical inverse problem, graph Laplacian operator, ill-posed problems, phase retrieval, medical imaging.

MSC codes: 47J06, 05C90, 92C50, 47A52.

1. INTRODUCTION

Inverse problems are encountered in various scientific and engineering disciplines, with the objective being to determine an unknown value from indirect and noisy data. Examples include image reconstruction in medical tomography [8], parameter identification in PDEs [25], and signal recovery in geophysics [35]. Mathematically, these problems are often cast as linear or nonlinear operator equations of the type

$$(1) \quad \mathcal{F}(u) = v,$$

where $\mathcal{F} : \mathcal{D}(\mathcal{F}) \subset \mathcal{U} \simeq \mathbb{R}^n \rightarrow \mathcal{V} \simeq \mathbb{R}^m$ represents the forward operator mapping the solution space \mathcal{U} to the data space \mathcal{V} . Here, \mathcal{U} and \mathcal{V} possess the canonical inner product $\langle \cdot, \cdot \rangle$ and induced norm $\|\cdot\|$. In practical scenarios, the exact data v is unavailable and only noisy measurement v^δ can be observed. Due to their ill-posed nature, inverse problems (1) are highly sensitive to data perturbations, making the stable recovery of the true solution from noisy observations a central computational

Department of Mathematics, Indian Institute of Technology Roorkee, Roorkee, Uttarakhand 247667, India.

E-mail: harshit_b@ma.iitr.ac.in (Harshit Bajpai), ankik.giri@ma.iitr.ac.in (Ankik Kumar Giri).

This work was supported by the Anusandhan National Research Foundation (ANRF), India, under Grant No. CRG/2022/00548.

challenge. When the noise level $\delta = \|v - v^\delta\|$ is known, various variational [46] and iterative regularization methods [34] have been created. Among them, Landweber-type schemes [17, 19, 30, 41, 44] have attracted extensive study. Recently, data-driven regularization [2, 3, 6, 50] has gained prominence for incorporating *a priori* information. In a similar spirit, graph-based regularization methods [5, 9, 10] have emerged for linear ill-posed problems, where a graph constructed from the signal encodes essential features of the ground truth via the associated graph Laplacian which is employed as a guiding operator within the regularization framework.

As demonstrated in [39], imaging tasks like deblurring and tomography perform poorly when the graph \mathcal{G} is constructed directly from noisy data v^δ , since v^δ resides in a different space from the ground-truth image u^\dagger . In order to solve this problem, the authors suggested a preprocessing step that maps the data through a reconstruction operator $\Psi : \mathcal{V} \rightarrow \mathcal{U}$, and the graph is then constructed from $\Psi(v^\delta)$. The operator Ψ transfers information from the measurement space to the solution space and can be implemented, for instance, using Tikhonov filtering [14] or filtered back-projection (FBP) [33]. Building on [39], the work in [10] proposed a graph-based variational regularization method, denoted as `graphLa+ Ψ` , which was later extended in [5] to an iterative method equipped with an *a posteriori* stopping rule, thereby alleviating the computational challenges of variational formulations. In these frameworks, preprocessing is performed via a family of reconstruction operators $\Psi_\Theta : \mathcal{V} \rightarrow \mathcal{U}$, parameterized by $\Theta = \Theta(\delta, v^\delta)$, where the parameters may depend on both the noise level and the observed data. The pair (Ψ_Θ, Θ) is defined in a general and flexible setting, without the requirement that it constitutes a convergent regularization method.

While iterative methods are effective for addressing ill-posed inverse problems, their inherent semi-convergence behavior necessitates an appropriate stopping criterion to prevent overfitting to noise. A conventional choice is the *discrepancy principle* [42], which guarantees regularization when the noise level δ is known. However, in many practical scenarios, accurately estimating δ is infeasible. To address this limitation, *heuristic stopping rules* [4, 29, 37, 45] have been developed, which determine the stopping index directly from the noisy data v^δ without requiring explicit noise information. Empirical studies indicate that these rules can perform on par with, or even surpass, methods relying on explicit noise knowledge, though they often require restrictive assumptions on the noise structure. Alternatively, averaging multiple unbiased measurements has been explored to approximate stable solutions, as systematically analyzed in [21, 22, 26, 31] for linear regularization methods with unknown noise in Hilbert spaces.

Graph-based regularization methods have demonstrated promising potential in imaging and related applications, yet the field remains in its early stages, offering promising direction for advancement. Motivated by this, the present work extends the graph-based iterative regularization framework (`IRMGL+ Ψ`) [5] along four key directions. First, we generalize the approach beyond the linear setting to handle nonlinear ill-posed problems under suitable assumptions, thereby broadening both its theoretical foundation and practical applicability. Second, we introduce a heuristic stopping rule that depends solely on the observed data, eliminating the need for prior noise knowledge. To address its limitations, we further develop a statistical discrepancy principle, derived empirically yet likewise independent of explicit noise information. Both stopping criteria exploit repeated noisy measurements, which form a central element of our design. Finally, to validate the proposed approach, we carry out comprehensive numerical experiments on both X-ray CT and phase retrieval CT problems. These experiments are designed to examine and compare the behavior of the proposed method under two different stopping rules. The results demonstrate superior reconstruction accuracy and stability, underscoring the potential of the proposed framework to advance modern imaging techniques in scientific and medical applications.

To realize this idea, we assume that measurements can be repeatedly acquired under identical experimental conditions, while the true underlying solution remains fixed. This setting aligns with the well-established engineering practice of *signal averaging*, which leverages repeated measurements to mitigate random errors (see [40] for an introduction and [23] for a comprehensive survey).

Accordingly, we consider a sequence of independent and identically distributed \mathcal{V} -valued random variables v_1, v_2, \dots , within the probability space $(\Omega, \mathbb{F}, \mathbb{P})$, each serving as an unbiased observation of the exact but unknown data v . For any $m \geq 1$, we define the mean

$$(2) \quad \hat{v}^{(m)} := \frac{1}{m} \sum_{i=1}^m v_i,$$

which provides an estimator of v . Let $\mathbb{E}[\cdot]$ denote the expectation and assuming that $\mathbb{E}[v_1] = v$ with

$$0 < \sigma^2 := \mathbb{E}[\|v_1 - v\|^2] < \infty,$$

it follows that

$$\mathbb{E}[\|\hat{v}^{(m)} - v\|^2] = \frac{\sigma^2}{m}.$$

Hence, averaging over m independent measurements reduces the variance σ^2 by a factor of m , yielding a progressively more accurate approximation of the true data as $m \rightarrow \infty$.

Building upon the above framework of empirical averaging, we develop a novel and enhanced iterative regularization scheme assisted by the graph Laplacian, referred to as **E-IRMGL+ Ψ** . In this approach, the empirical mean $\hat{v}^{(m)}$ serves as the input data for the reconstruction process. As a preliminary step, we introduce a family of reconstruction mappings

$$\Psi_\theta : \mathcal{V} \rightarrow \mathcal{U},$$

where the parameter $\theta := \theta(m, \hat{v}^{(m)})$ may depend on both the number of measurements m and the averaged data $\hat{v}^{(m)}$. The proposed iterative scheme is then formulated as

$$(3) \quad \begin{cases} u_{k+1}^{(m)} = u_k^{(m)} - \alpha_k^{(m)} \mathcal{F}'(u_k^{(m)})^* (\mathcal{F}(u_k^{(m)}) - \hat{v}^{(m)}) - \beta_k^{(m)} \Delta_{u_k^{(m)}} u_k^{(m)}, \\ u_0^{(m)} = \Psi_\theta(\hat{v}^{(m)}), \end{cases}$$

where $k \geq 1$, $\mathcal{F}'(u_k^{(m)})^*$ denotes the adjoint of the Fréchet derivative $\mathcal{F}'(u_k^{(m)})$, Δ_u is the data-dependent graph Laplacian constructed from u (for further information, see Subsection 2.1), and $\alpha_k^{(m)} > 0$ and $\beta_k^{(m)} \geq 0$ denote the step size and regularization weight, respectively. A comprehensive discussion of the method's formulation, theoretical properties, and computational aspects is provided in Section 2 and Subsection 3.1, while a schematic illustration of the overall method is shown in Fig. 1. It is important to note that the iteration in (3) can be interpreted as a gradient descent method applied to the functional

$$\mathcal{J}(u) := \frac{1}{2} \left(\|\mathcal{F}(u) - \hat{v}^{(m)}\|^2 + \beta \langle u, \Delta_u u \rangle \right),$$

where $\beta \geq 0$ is a regularization parameter. The first term enforces data fidelity by penalizing the discrepancy between the model output $\mathcal{F}(u)$ and the measured data $\hat{v}^{(m)}$. The second term acts as a graph-based regularizer that incorporates structural information encoded in the graph Laplacian Δ_u . Computing the Fréchet derivative of \mathcal{J} with respect to u yields

$$\nabla \mathcal{J}(u) = \mathcal{F}'(u)^* (\mathcal{F}(u) - \hat{v}^{(m)}) + \beta \Delta_u u.$$

Thus, a gradient descent update with step size $\alpha_k^{(m)} > 0$ naturally leads to

$$u_{k+1}^{(m)} = u_k^{(m)} - \alpha_k^{(m)} (\mathcal{F}'(u_k^{(m)})^* (\mathcal{F}(u_k^{(m)}) - \hat{v}^{(m)}) + \beta \Delta_{u_k^{(m)}} u_k^{(m)}),$$

which coincides with the scheme defined in (3), after allowing the parameters $\alpha_k^{(m)}$ and $\beta_k^{(m)}$ to vary across iterations. Hence, the proposed method can be rigorously viewed as a graph-regularized gradient descent for minimizing $\mathcal{J}(u)$.

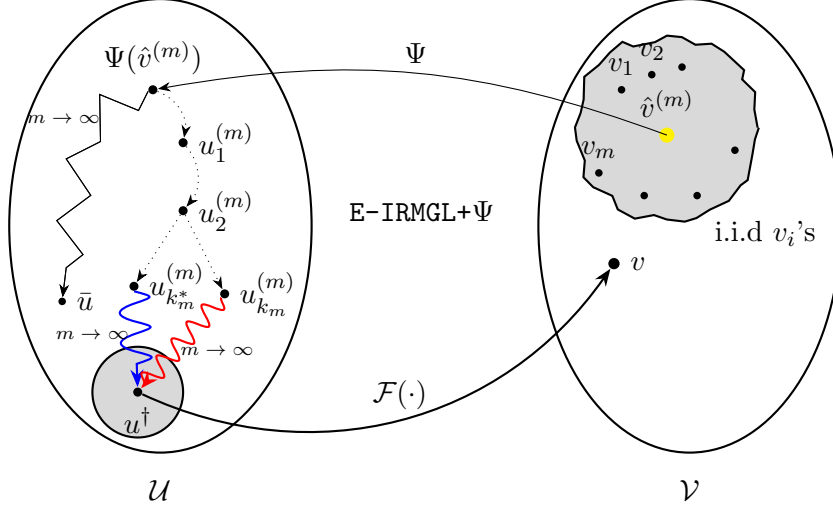


FIGURE 1. A schematic representation of the E-IRMGL+ Ψ approach with two noise level free stopping rules. Independent and identically distributed samples v_1, v_2, \dots, v_m (black points near $\hat{v}^{(m)}$) are averaged to obtain $\hat{v}^{(m)}$ (yellow). The primary reconstructor Ψ is not usually a regularization technique, which is reflected in the piecewise linear trajectory of $\Psi(\hat{v}^{(m)})$ as $m \rightarrow \infty$. Starting from $\Psi(\hat{v}^{(m)})$, the iterative procedure generates approximations $u_k^{(m)}$. The approximate reconstructions obtained via the heuristic and statistical stopping rules are denoted by $u_{k_m^*}^{(m)}$ and $u_{k_m}^{(m)}$, respectively. As $m \rightarrow \infty$, both sequences converge to the ground-truth solution u^\dagger . The convergence of $u_{k_m^*}^{(m)}$ is indicated by the blue coiled arrow, whereas the convergence of $u_{k_m}^{(m)}$ is represented by the red wavy arrow.

The convergence analysis in this work differs significantly from existing studies [5, 10]. First, the use of multiple repeated measurements requires stochastic techniques, in contrast to the deterministic settings of [5, 10]. Second, the regularization term depends explicitly on both the empirical mean and the number of measurements m , adding complexity to the stability analysis and necessitating mild but essential assumptions. Third, to our knowledge, this is the first study to examine heuristic and statistical stopping rules within graph-based regularization. These advancements together constitute the main novel contributions of this work.

The paper is organized as follows. Section 2 begins with the essential definitions and preliminaries, followed by the key assumptions of the study. The section then introduces the heuristic and statistical stopping strategies that constitute the main components of the proposed framework. Section 3 presents the algorithmic formulation under the statistical stopping rule and establishes stability and convergence results. Section 4 develops the algorithm under heuristic stopping rule and its convergence analysis. The performance of the proposed approach, along with a comparison of both stopping rules, is demonstrated through numerical experiments in Section 5. Finally, Section 6 summarizes the main contributions and outlines future research directions.

2. THE E-IRMGL+ Ψ METHOD

In this section, we investigate the iterative scheme introduced in (3) and provide a comprehensive description. Two stopping rules, formulated independently of any *a priori* knowledge of the noise level, are introduced. We begin by recalling essential notions from graph theory and their connection to image representations (see [36] for a modern introduction).

2.1. Images and graphs.

Definition 2.1. Let $\mathcal{S} = \{a_1, a_2, \dots, a_{|\mathcal{S}|}\}$ be a finite set, $|\mathcal{S}|$ being its cardinality. A graph over \mathcal{S} is a pair $\mathcal{G} = (\mathcal{S}, e_w)$, where $e_w : \mathcal{S} \times \mathcal{S} \rightarrow [0, \infty)$ is an edge-weight function satisfying

- Symmetry: $e_w(a, b) = e_w(b, a)$ for all $a, b \in \mathcal{S}$,
- No self-loops: $e_w(a, a) = 0$ for all $a \in \mathcal{S}$.

The edge set is $T := \{(a, b) \in \mathcal{S} \times \mathcal{S} \mid e_w(a, b) \neq 0\}$. Nodes $a, b \in \mathcal{S}$ are connected, denoted $a \sim b$, if $e_w(a, b) > 0$, where $e_w(a, b)$ quantifies the strength of their connection.

Definition 2.2. For any function $\mathbf{u} : \mathcal{S} \rightarrow \mathbb{R}$, the graph Laplacian $\Delta \mathbf{u} : \mathcal{S} \rightarrow \mathbb{R}$ is defined by

$$(4) \quad \Delta \mathbf{u}(a) := \sum_{a \sim b} e_w(a, b) (\mathbf{u}(a) - \mathbf{u}(b)).$$

In matrix form,

$$(5) \quad \Delta = D - W,$$

where D denotes the diagonal degree matrix with entries $d_{ii} = \sum_{j=1}^{|\mathcal{S}|} e_w(a_i, a_j)$ and $W = [e_w(a_i, a_j)]_{i,j=1}^{|\mathcal{S}|}$ is the weight matrix.

The operator in (5) coincides with the action in (4). Note that, defining a graph requires specifying a set of nodes \mathcal{S} together with an edge-weight function e_w . We now describe how such a graph can be constructed from an image.

An image can be viewed as a grid of pixels $a \in \mathcal{S}$, where each pixel is indexed by $a = (i_a, j_a)$ with $i_a \in \{1, \dots, p\}$ and $j_a \in \{1, \dots, q\}$, denotes its horizontal and vertical axes, respectively. Thus, the node set can be written as

$$\mathcal{S} := \{a = (i_a, j_a) : i_a \in \{1, \dots, p\}, j_a \in \{1, \dots, q\}\}.$$

For the sake of keeping things simple, we take grayscale images, represented as function $\mathbf{u} : \mathcal{S} \rightarrow [0, 1]$, assigning an intensity to each pixel, where 0 and 1 correspond to black and white, respectively, and intermediate values denote shades of gray. A common approach to define the edge weight between two pixels incorporates both spatial proximity and intensity similarity is

$$(6) \quad e_{w\mathbf{u}}(a, b) = g(a, b) h_{\mathbf{u}}(a, b),$$

where $g(a, b)$ captures the geometric relationship of \mathcal{S} , typically

$$g(a, b) = \mathbf{1}_{(0, R]}(d(a, b)),$$

with $R > 0$ controlling the neighborhood radius, $\mathbf{1}_{(0, R]}$ the indicator function, and $d(a, b)$ a distance metric (e.g., $d(a, b) = |i_a - i_b| + |j_a - j_b|$ or $d(a, b) = \max\{|i_a - i_b|, |j_a - j_b|\}$). The function $h_{\mathbf{u}}(a, b)$ accounts for intensity similarity, commonly using a Gaussian kernel

$$h_{\mathbf{u}}(a, b) = \exp\left(-\frac{|\mathbf{u}(a) - \mathbf{u}(b)|^2}{\lambda}\right), \quad \lambda > 0.$$

For detailed discussions on constructing graph weights from grayscale images using such kernels, see [9, 10, 12, 13, 18, 39]. Assume that $R < \infty$. Then, each node $a \in \mathcal{S}$ is connected to at most D_N neighboring nodes, i.e.,

$$\deg(a) := \#\{b \in \mathcal{S} : g(a, b) \neq 0\} \leq D_N, \quad \text{for all } a \in \mathcal{S},$$

where $\deg(a)$ denotes the degree of node a .

2.2. Assumptions and stopping rules. In this subsection, we first introduce some necessary assumptions which are essential for the subsequent analysis.

Assumption 2.3. For every $u, w \in \mathcal{B}_{3\varphi}(u_0^{(m)}) \subset \mathcal{D}(\mathcal{F})$, the following properties hold, where $\mathcal{B}_\varphi(u_0^{(m)})$ denotes the closed ball of radius φ centered at $u_0^{(m)}$.

- (A1) The operator \mathcal{F} is Fréchet differentiable with derivative $\mathcal{F}'(u)$. Moreover, the mapping $u \mapsto \mathcal{F}'(u)$ is continuous.
- (A2) The derivatives are uniformly bounded, i.e., $\|\mathcal{F}'(u)\| \leq B$, for some constant $B > 0$ independent of u .
- (A3) (**Tangential cone condition**) There exists a constant $\eta \in [0, 1)$ such that

$$\|\mathcal{F}(u) - \mathcal{F}(w) - \mathcal{F}'(w)(u - w)\| \leq \eta \|\mathcal{F}(u) - \mathcal{F}(w)\|$$

- (A4) There exists a constant $L \geq 0$ such that

$$\|\mathcal{F}'(u) - \mathcal{F}'(w)\| \leq L \|u - w\|.$$

- (A5) There exists $u^\dagger \in \mathcal{B}_\varphi(u_0^{(m)})$ such that $\mathcal{F}(u^\dagger) = v$.

In Assumption 2.3, conditions (A1) and (A2) ensure that the derivative $\mathcal{F}'(u)$ is locally bounded and continuous within the closed ball $\mathcal{B}_{3\varphi}(u_0^{(m)})$. When \mathcal{F} is a bounded linear operator, conditions (A1)–(A4) of Assumption 2.3 are automatically satisfied with $\eta = 0$. In the nonlinear setting, condition (A3) imposes a restriction on the degree of nonlinearity of \mathcal{F} , and this assumption has been verified for various classes of nonlinear inverse problems [19]. Condition (A4) corresponds to the well-known notion of L -smoothness, which requires that the derivative $\mathcal{F}'(u)$ is uniformly controlled by a parameter, thereby preventing arbitrary variations. This property plays a fundamental role in establishing convergence guarantees for most gradient-type methods [11] and has been extensively validated in practical applications [32].

Remark 2.4. The condition (A5) of the aforementioned assumption guarantees that the exact solution u^\dagger is in close proximity to the initial reconstruction $u_0^{(m)} = \Psi_\theta(\hat{v}^{(m)})$, and is compatible with the forward model. For several standard choices of the reconstruction operator Ψ_θ , this assumption is naturally satisfied. For instance, when Ψ_θ is chosen to be the Tikhonov regularizer, i.e.,

$$\Psi_\theta^{\text{Tik}}(\hat{v}^{(m)}) = \arg \min_{u \in \mathcal{D}(\mathcal{F})} \left\{ \frac{1}{2} \|\mathcal{F}(u) - \hat{v}^{(m)}\|^2 + \frac{\theta}{2} \|u\|^2 \right\},$$

where $\theta := \theta(m, \hat{v}^{(m)})$ is the regularization parameter. It follows from the fact that, under standard assumptions Tikhonov regularization along with the appropriate regularization parameter θ becomes a convergent regularization method. Consequently, for sufficiently small values of θ , the exact solution u^\dagger lies within the ball $\mathcal{B}_\varphi(u_0^{(m)})$ for a suitably chosen radius $\varphi > 0$. Further technical details can be found in [5].

Building upon these structural conditions, we next impose assumptions on the measurement data.

Assumption 2.5. Let $\{v_i\}_{i \geq 1}$ be a sequence of i.i.d. \mathcal{V} -valued random variables defined on a probability space $(\Omega, \mathbb{F}, \mathbb{P})$. We assume that they are unbiased with $\mathbb{E}[v_1] = v$, and possess finite, nonzero variance

$$0 < \sigma^2 := \mathbb{E}[\|v_1 - v\|^2] < \infty.$$

Then, for the empirical mean (2) we obtain

$$\mathbb{E}[\|\hat{v}^{(m)} - v\|^2] = \frac{1}{m^2} \sum_{i,j=1}^m \mathbb{E}[\langle v_i - v, v_j - v \rangle] = \frac{1}{m^2} \sum_{i=1}^m \mathbb{E}[\|v_i - v\|^2] = \frac{\sigma^2}{m}.$$

This calculation shows that the variance is reduced by a factor of m . Consequently, it is reasonable to expect that using the averaged data $\hat{v}^{(m)}$ yields a more accurate approximation of v than relying on any single observation v_i .

Next, we introduce a heuristic stopping rule for the E-IRMGL+ Ψ method (3) that does not rely on the noise level but instead utilizes empirical information derived from the measurement data. The proposed rule is motivated by the ideas in [20, 37].

Rule 1 (Heuristic principle). Let $\varrho \geq 1$ and let

$$\Omega(k, \hat{v}^{(m)}) := (k + \varrho) \left\| \mathcal{F}(u_k^{(m)}) - \hat{v}^{(m)} \right\|^2.$$

Define $k_m^* := k_m^*(\hat{v}^{(m)})$ is an integer satisfying

$$k_m^* \in \arg \min \left\{ \Omega(k, \hat{v}^{(m)}) : k \in [0, k_\infty] \right\},$$

where $k_\infty := k_\infty(\hat{v}^{(m)})$ is the largest integer such that $u_k^{(m)} \in \mathcal{D}(\mathcal{F})$ for all $k \in [0, k_\infty]$.

Bakushinskii's veto [7] asserts that heuristic stopping rules cannot guarantee convergence in the worst-case setting for any regularization method. Nevertheless, under additional assumptions on the noise, convergence of heuristic rules has been established for several regularization approaches [4, 16, 20, 27, 28, 29, 38, 45, 49]. Motivated by the studies [20, 28], we adopt a similar condition in the context of measurement data and formulate the following assumption.

Assumption 2.6. *There exists a constant $\kappa > 0$, independent of m , such that with high probability*

$$\|\hat{v}^{(m)} - \mathcal{F}(u)\| \geq \kappa \|\hat{v}^{(m)} - v\|$$

for every $u \in S(\hat{v}^{(m)}) := \{u_k^{(m)} : k \in [0, k_\infty]\}$, where $\{u_k^{(m)}\}$ is the sequence generated by E-IRMGL+ Ψ (3).

Remark 2.7. The above assumption guarantees that the residual $\|\hat{v}^{(m)} - \mathcal{F}(u)\|$ does not fall significantly below $\|\hat{v}^{(m)} - v\|$, thereby preventing degenerate noise realizations. Although this condition cannot be verified in practice, it is essential to circumvent Bakushinskii's veto [7] and is standard in the analysis of heuristic parameter choice rules [4, 27, 29, 37, 45]. Its practical validity is typically supported by numerical evidence; see [24] for a detailed study in the context of nonlinear Landweber iteration.

To address the shortcomings of Assumption 2.6, we also introduce a stopping rule that leverages the average over multiple unbiased measurements. Recall that

$$\mathbb{E}[\|\hat{v}^{(m)} - v\|^2] = \frac{\sigma^2}{m}.$$

To estimate σ^2 , we consider the empirical variance

$$(7) \quad z_m^2 := \frac{1}{m-1} \sum_{i=1}^m \|v_i - \hat{v}^{(m)}\|^2,$$

which satisfies $\mathbb{E}[z_m^2] = \sigma^2$ (cf. Assumption 2.5). Thus, z_m^2 serves as an unbiased estimator of the variance σ^2 , a standard fact in statistics (see also [21, 31]). Consequently, we may use z_m/\sqrt{m} as an estimator of $\|\hat{v}^{(m)} - v\|$. This motivates the following statistical variant of the discrepancy principle, see [31, 48].

Rule 2 (Statistical discrepancy principle). Define k_m as the first integer satisfying

$$(8) \quad \left\| \mathcal{F}(u_{k_m}^{(m)}) - \hat{v}^{(m)} \right\| \leq \frac{\tau_m}{\sqrt{m}} z_m,$$

where $\tau_m > 1$ may depend on m .

It is worth emphasizing that, unlike the deterministic stopping index in the classical discrepancy principle [42] and the Hanke–Raus heuristic rule [45], the stopping indices k_m^* and k_m determined by rule 1 and rule 2 are inherently *random variables*. Consequently, their analysis necessitates the use of statistical tools. So, for the convergence analysis of E-IRMGL+ Ψ (3) under these two stopping rules, a key step is the construction of an event Γ_m satisfying $\mathbb{P}(\Gamma_m) \rightarrow 1$ as $m \rightarrow \infty$, in line with the arguments of [21, 31]. For technical reasons, the subsequent regularization analysis requires that

$$\tau_m \rightarrow \infty \quad \text{and} \quad \frac{\tau_m}{\sqrt{m}} \rightarrow 0 \quad \text{as } m \rightarrow \infty.$$

Accordingly, we define

$$\Gamma_m := \left\{ |z_m - \sigma| \leq \frac{\sigma}{2}, \quad \|\hat{v}^{(m)} - v\| \leq \frac{\tau_m}{\mathcal{H}\sqrt{m}} z_m \right\},$$

where

$$\mathcal{H} > \frac{1+\eta}{1-\eta}$$

with $\eta \in [0, 1)$. On this event, the subsequent convergence analysis will be carried out. With this construction, one can obtain

$$\mathbb{P}(\Gamma_m) \rightarrow 1 \quad \text{as } m \rightarrow \infty.$$

3. CONVERGENCE ANALYSIS UNDER STATISTICAL DISCREPANCY PRINCIPLE

In this section, we aim to establish the regularization property of the proposed E-IRMGL+ Ψ method with multiple repeated measurements, when terminated using rule 2.

3.1. The method. We begin by providing a detailed exposition of the method. To this end, we introduce the step size $\alpha_k^{(m)}$ and the weight parameter $\beta_k^{(m)}$, which are designed to enhance the speed of convergence of (3). A natural strategy is to select $\alpha_k^{(m)}$ and $\beta_k^{(m)}$ at each iteration so that the generated sequence remains sufficiently close to a solution of (1). Based on this principle, we define the parameters as

$$(9) \quad 0 < \zeta \leq \alpha_k^{(m)} = \min \left\{ \frac{\zeta_0 \|\mathcal{F}(u_k^{(m)}) - \hat{v}^{(m)}\|}{\|\mathcal{F}'(u_k^{(m)})^*(\mathcal{F}(u_k^{(m)}) - \hat{v}^{(m)})\|}, \zeta_1 \right\},$$

$$(10) \quad \beta_k^{(m)} = \begin{cases} \min \left\{ \frac{\nu_0 \|\mathcal{F}(u_k^{(m)}) - \hat{v}^{(m)}\|^2}{\|\Delta_{u_k^{(m)}} u_k^{(m)}\|^2}, \frac{\nu_1}{\|\Delta_{u_k^{(m)}} u_k^{(m)}\|}, \nu_2 \right\}, & \text{if } \|\Delta_{u_k^{(m)}} u_k^{(m)}\| \neq 0 \\ 0, & \text{if } \|\Delta_{u_k^{(m)}} u_k^{(m)}\| = 0, \end{cases}$$

where $\zeta_0, \zeta_1, \nu_0, \nu_1$ and ν_2 denotes the fixed positive constants. We impose the following condition

$$\zeta > \frac{\nu_0(\varphi + \nu_1) + \zeta_0^2}{1 - \eta - \frac{1+\eta}{\mathcal{H}}}.$$

This choice will later play a crucial role in ensuring the positivity of the constant introduced in (11). The pseudo-code for the iterative scheme (3), when stopped using rule 2, is given in Algorithm 1, where at each iteration the graph Laplacian $\Delta_{u_k^{(m)}}$ is reconstructed from the current iterate $u_k^{(m)}$, ensuring adaptive updating of the regularization term throughout the process.

The following result establishes key properties of the iterates from Algorithm 1, which are crucial for proving finite termination of the scheme.

Algorithm 1 E-IRMGL+ Ψ with statistical discrepancy principle

- 1: **Input:** Operator \mathcal{F} , measurements v_1, v_2, \dots, v_m , initial reconstructor Ψ_θ , parameters θ, λ, R , and $\tau_m > 1$.
- 2: **Set:** $\hat{v}^{(m)} := \frac{1}{m} \sum_{i=1}^m v_i$ and $z_m := \sqrt{\frac{1}{m-1} \sum_{i=1}^m \|v_i - \hat{v}^{(m)}\|^2}$.
- 3: **Initialize:** $u_0^{(m)} := \Psi_\theta(\hat{v}^{(m)})$.
- 4: **while** $\|\mathcal{F}(u_k^{(m)}) - \hat{v}^{(m)}\| > \frac{\tau_m}{\sqrt{m}} z_m$ **do**
- 5: Compute $\Delta_{u_k^{(m)}}$ from $u_k^{(m)}$, R , and λ as defined in (4).
- 6: Update the iterate

$$u_{k+1}^{(m)} := u_k^{(m)} - \alpha_k^{(m)} \mathcal{F}'(u_k^{(m)})^* (\mathcal{F}(u_k^{(m)}) - \hat{v}^{(m)}) - \beta_k^{(m)} \Delta_{u_k^{(m)}} u_k^{(m)},$$

where $\alpha_k^{(m)}$ and $\beta_k^{(m)}$ are given by (9) and (10).
- 7: **end while**
- 8: **Output:** $u_{k_m}^{(m)}$.

Lemma 3.1. Suppose that Assumptions 2.3 and 2.5 hold. Let the sequence $\{u_k^{(m)}\}$ be generated by Algorithm 1, and let k_m denote the stopping index defined by the statistical discrepancy principle (see rule 2). Assume that

$$(11) \quad \mathcal{C} := \left(1 - \eta - \frac{1+\eta}{\mathcal{H}}\right) \zeta - \nu_0(\varphi + \nu_1) - \zeta_0^2 > 0.$$

For any integer $n \leq k_m$, the following statements hold:

(i) **Monotonicity:** For all $0 \leq k < n$,

$$\|u_{k+1}^{(m)} - u^\dagger\| \leq \|u_k^{(m)} - u^\dagger\|.$$

(ii) **Stability and residual control:** The iterates satisfy $u_k^{(m)} \in \mathcal{B}_\varphi(u^\dagger)$ for all $0 \leq k \leq n$, and

$$\sum_{k=0}^n \|\mathcal{F}(u_k^{(m)}) - \hat{v}^{(m)}\|^2 \leq \frac{1}{2\mathcal{C}} \|u_0^{(m)} - u^\dagger\|^2.$$

Proof. By condition (A5) in Assumption 2.3, the initial iterate satisfies $u_0^{(m)} \in \mathcal{B}_\varphi(u^\dagger)$. Assume further that $u_k^{(m)} \in \mathcal{B}_\varphi(u^\dagger)$ for some iteration index k . It then follows that $u_k^{(m)} \in \mathcal{B}_{2\varphi}(u_0^{(m)})$. We now define

$$g_k^{(m)} := u_k^{(m)} - u^\dagger \quad \text{and} \quad h_k^{(m)} := \alpha_k^{(m)} \mathcal{F}'(u_k^{(m)})^* (\mathcal{F}(u_k^{(m)}) - \hat{v}^{(m)}) + \beta_k^{(m)} \Delta_{u_k^{(m)}} u_k^{(m)}.$$

With these definitions in place, and by applying the update rule from Algorithm 1, we obtain

$$(12) \quad \|g_{k+1}^{(m)}\|^2 - \|g_k^{(m)}\|^2 = \|h_k^{(m)}\|^2 - 2\langle g_k^{(m)}, h_k^{(m)} \rangle.$$

Our next step is to examine the two terms on the right-hand side of (12). To begin, we consider the first term. By using the definitions of $\alpha_k^{(m)}$ and $\beta_k^{(m)}$, we obtain

$$\begin{aligned}
\|h_k^{(m)}\|^2 &= \|\alpha_k^{(m)} \mathcal{F}'(u_k^{(m)})^* (\mathcal{F}(u_k^{(m)}) - \hat{v}^{(m)}) + \beta_k^{(m)} \Delta_{u_k^{(m)}} u_k^{(m)}\|^2 \\
&\leq 2\zeta_0^2 \|\mathcal{F}(u_k^{(m)}) - \hat{v}^{(m)}\|^2 + 2\nu_0\nu_1 \|\mathcal{F}(u_k^{(m)}) - \hat{v}^{(m)}\|^2 \\
(13) \quad &\leq 2(\zeta_0^2 + \nu_0\nu_1) \|\mathcal{F}(u_k^{(m)}) - \hat{v}^{(m)}\|^2.
\end{aligned}$$

Similarly, by utilizing (A3) of Assumption 2.3, we have the estimate for the second term as

$$\begin{aligned}
-\langle g_k^{(m)}, h_k^{(m)} \rangle &= \alpha_k^{(m)} \langle \mathcal{F}'(u_k^{(m)})(u^\dagger - u_k^{(m)}), \mathcal{F}(u_k^{(m)}) - \hat{v}^{(m)} \rangle - \beta_k^{(m)} \langle g_k^{(m)}, \Delta_{u_k^{(m)}} u_k^{(m)} \rangle \\
&= \alpha_k^{(m)} \langle \mathcal{F}(u_k^{(m)}) - \hat{v}^{(m)} + \mathcal{F}'(u_k^{(m)})(u^\dagger - u_k^{(m)}), \mathcal{F}(u_k^{(m)}) - \hat{v}^{(m)} \rangle \\
&\quad - \alpha_k^{(m)} \langle \mathcal{F}(u_k^{(m)}) - \hat{v}^{(m)}, \mathcal{F}(u_k^{(m)}) - \hat{v}^{(m)} \rangle + \beta_k^{(m)} \wp \|\Delta_{u_k^{(m)}} u_k^{(m)}\| \\
&= \alpha_k^{(m)} \|\mathcal{F}(u_k^{(m)}) - \hat{v}^{(m)}\| \left[\eta \|\mathcal{F}(u_k^{(m)}) - \hat{v}^{(m)}\| + (1 + \eta) \|v - \hat{v}^{(m)}\| \right] \\
&\quad - \alpha_k^{(m)} \|\mathcal{F}(u_k^{(m)}) - \hat{v}^{(m)}\|^2 + \beta_k^{(m)} \wp \|\Delta_{u_k^{(m)}} u_k^{(m)}\| \\
&\leq -(1 - \eta) \alpha_k^{(m)} \|\mathcal{F}(u_k^{(m)}) - \hat{v}^{(m)}\|^2 + \wp \nu_0 \|\mathcal{F}(u_k^{(m)}) - \hat{v}^{(m)}\|^2 \\
&\quad + (1 + \eta) \alpha_k^{(m)} \|v - \hat{v}^{(m)}\| \|\mathcal{F}(u_k^{(m)}) - \hat{v}^{(m)}\|.
\end{aligned}$$

In deriving the last inequality, we have made use of (10). Since $k < n \leq k_m$, it follows that

$$\|\mathcal{F}(u_k^{(m)}) - \hat{v}^{(m)}\| > \frac{\tau_m}{\sqrt{m}} z_m.$$

Furthermore, from the properties of the space Γ_m , we obtain

$$\|v - \hat{v}^{(m)}\| \leq \frac{\tau_m}{\mathcal{H} \sqrt{m}} z_m.$$

Combining these observations yields the bound

$$(14) \quad -\langle g_k^{(m)}, h_k^{(m)} \rangle \leq -\left(1 - \eta - \frac{1 + \eta}{\mathcal{H}}\right) \alpha_k^{(m)} \|\mathcal{F}(u_k^{(m)}) - \hat{v}^{(m)}\|^2 + \wp \nu_0 \|\mathcal{F}(u_k^{(m)}) - \hat{v}^{(m)}\|^2.$$

By substituting (13) and (14) into (12), we obtain

$$(15) \quad \|g_{k+1}^{(m)}\|^2 - \|g_k^{(m)}\|^2 \leq -2 \left[\left(1 - \eta - \frac{1 + \eta}{\mathcal{H}}\right) \zeta - \nu_0 (\wp + \nu_1) - \zeta_0^2 \right] \|\mathcal{F}(u_k^{(m)}) - \hat{v}^{(m)}\|^2.$$

Finally, substituting (11) into (15) yields

$$(16) \quad \|g_{k+1}^{(m)}\|^2 - \|g_k^{(m)}\|^2 \leq -2\mathcal{C} \|\mathcal{F}(u_k^{(m)}) - \hat{v}^{(m)}\|^2.$$

Thus, the monotonicity holds for $0 \leq k < n$.

Next, we turn to the proof of assertion (ii). The inequality (16) ensures that

$$\|u_{k+1}^{(m)} - u^\dagger\| \leq \|u_k^{(m)} - u^\dagger\| \leq \wp,$$

which suggests that $u_{k+1}^{(m)} \in \mathcal{B}_\wp(u^\dagger)$. From $k = 0$ to $k = n$, the inequality (16) can be summed to produce

$$(17) \quad \sum_{k=0}^n \left[\|g_{k+1}^{(m)}\|^2 - \|g_k^{(m)}\|^2 \right] \leq -2\mathcal{C} \sum_{k=0}^n \|\mathcal{F}(u_k^{(m)}) - \hat{v}^{(m)}\|^2.$$

In conclusion, (17) implies that

$$\sum_{k=0}^n \|\mathcal{F}(u_k^{(m)}) - \hat{v}^{(m)}\|^2 \leq \frac{1}{2\mathcal{C}} \|g_0^{(m)}\|^2 = \frac{1}{2\mathcal{C}} \|u_0^{(m)} - u^\dagger\|^2.$$

This establishes the desired result. \square

The next result, shows the finite iteration termination property of Algorithm 1.

Theorem 3.2. *Given that the conditions of Lemma 3.1 hold, and Algorithm 1 is initialized with a starting point $u_0^{(m)}$. Then the algorithm exhibits finitely many iterations, i.e., there exist an integer $k_m < \infty$ such that*

$$\|\mathcal{F}(u_{k_m}^{(m)}) - \hat{v}^{(m)}\| \leq \frac{\tau_m}{\sqrt{m}} z_m < \|\mathcal{F}(u_k^{(m)}) - \hat{v}^{(m)}\|, \quad 0 \leq k < k_m.$$

Proof. Let n be a non-negative integer such that

$$\|\mathcal{F}(u_k^{(m)}) - \hat{v}^{(m)}\| > \frac{\tau_m}{\sqrt{m}} z_m \quad \forall k \in \{0, 1, \dots, n\}.$$

By invoking (17), yields

$$\begin{aligned} 2(n+1)\mathcal{C}\frac{\tau_m^2}{m} z_m^2 &\leq 2\mathcal{C} \sum_{k=0}^{k=n} \|\mathcal{F}(u_k^{(m)}) - \hat{v}^{(m)}\|^2 \leq \sum_{k=0}^{k=n} \left[\|g_k^{(m)}\|^2 - \|g_{k+1}^{(m)}\|^2 \right] \\ &= \|g_0^{(m)}\|^2 - \|g_{n+1}^{(m)}\|^2 \leq \|g_0^{(m)}\|^2. \end{aligned}$$

Taking expectations and using $\mathbb{E}[\|v - \hat{v}^{(m)}\|^2] = \frac{\sigma^2}{m} = \mathbb{E}\left[\frac{z_m^2}{m}\right]$, we obtain

$$2(n+1)\mathcal{C}\tau_m^2 \mathbb{E}[\|v - \hat{v}^{(m)}\|^2] \leq \|g_0^{(m)}\|^2 < \infty.$$

If no finite index k_m satisfied the stopping condition (8), then letting $n \rightarrow \infty$ in the above estimate would lead to a contradiction. Hence, Algorithm 1 must terminate after finitely many iterations. \square

3.2. Convergence for exact data. We examine Algorithm 1 without the superscript (m) in the case of exact data v . To establish convergence, it suffices to show that the sequence of iterates $\{u_k\}_{k \geq 0}$ forms a Cauchy sequence. We begin with a preliminary result on the behavior of $\{u_k\}_{k \geq 0}$.

Lemma 3.3. *Suppose that Assumption 2.3 hold, and let $\{u_k\}_{k \geq 0}$ denote the sequence generated by Algorithm 1 with exact data v . Then $u_k \in \mathcal{B}_\varphi(u^\dagger)$ for all $k \geq 0$, and*

$$(18) \quad \|u_{k+1} - u^\dagger\|^2 - \|u_k - u^\dagger\|^2 \leq -2\mathcal{C}_0 \|\mathcal{F}(u_k) - v\|^2, \quad \forall k \geq 0,$$

where $\mathcal{C}_0 := (1 - \eta)\zeta - \nu_0(\varphi + \nu_1) - \zeta_0^2 > 0$. Consequently, the sequence $\{\|u_k - u^\dagger\|\}_{k \geq 0}$ decreases monotonically, and

$$(19) \quad \sum_{k=0}^{\infty} \|\mathcal{F}(u_k) - v\|^2 \leq \frac{1}{2\mathcal{C}_0} \|u_0 - u^\dagger\|^2 < \infty,$$

where $u_0 := u_0^{(0)} = \Psi(v)$.

Proof. The assertion can be established through reasoning analogous to that employed in Lemma 3.1. \square

From (19), we deduce that for exact data the residual vanishes, i.e., $\|\mathcal{F}(u_k) - v\| \rightarrow 0$ as $k \rightarrow \infty$. This allows us to state the convergence result in the exact data setting.

Theorem 3.4. *Assuming the conditions of Lemma 3.3 are satisfied, the sequence of iterates $\{u_k\}_{k \geq 0}$ produced by the exact data version of Algorithm 1 converges to a solution, denoted u^\dagger , of the equation (1).*

Proof. For the exact data setting, define $g_k := u_k - u^\dagger$. Given indices $\ell \geq k$, select an integer m with $\ell \geq m \geq k$ in a way that

$$(20) \quad \|\mathcal{F}(u_m) - v\| \leq \|\mathcal{F}(u_n) - v\|, \quad \forall k \leq n \leq \ell.$$

By the triangle inequality, we obtain

$$(21) \quad \|g_\ell - g_k\| \leq \|g_\ell - g_m\| + \|g_m - g_k\|,$$

where the two terms admit the following expansions:

$$(22) \quad \|g_\ell - g_m\|^2 = 2\langle g_m - g_\ell, g_m \rangle + \|g_\ell\|^2 - \|g_m\|^2,$$

$$(23) \quad \|g_m - g_k\|^2 = 2\langle g_k - g_m, g_m \rangle + \|g_m\|^2 - \|g_k\|^2.$$

From Lemma 3.3, the sequence $\{\|g_k\|\}_{k \geq 0}$ is monotonically decreasing and bounded below by 0. Hence, the limit exists, say $\lim_{k \rightarrow \infty} \|g_k\| = \Theta \geq 0$. Consequently, we deduce

$$(24) \quad \lim_{k \rightarrow \infty} \|g_\ell - g_m\|^2 = 2 \lim_{k \rightarrow \infty} \langle g_m - g_\ell, g_m \rangle + \Theta^2 - \Theta^2,$$

$$(25) \quad \lim_{k \rightarrow \infty} \|g_m - g_k\|^2 = 2 \lim_{k \rightarrow \infty} \langle g_k - g_m, g_m \rangle + \Theta^2 - \Theta^2.$$

We want to show that $\{g_k\}_{k \geq 0}$ is a Cauchy sequence. Therefore, we assert that as $k \rightarrow \infty$, $\langle g_m - g_\ell, g_m \rangle \rightarrow 0$ and $\langle g_k - g_m, g_m \rangle \rightarrow 0$. In order to substantiate the assertion, it is evident that

$$\begin{aligned} |\langle g_m - g_\ell, g_m \rangle| &= |\langle u_m - u_\ell, g_m \rangle| = \left| \sum_{j=m}^{\ell-1} \langle u_{j+1} - u_j, g_m \rangle \right| \\ &\leq \left| \left\langle \sum_{j=m}^{\ell-1} (\alpha_j \mathcal{F}'(u_j)^*(\mathcal{F}(u_j) - v) + \beta_j \Delta_{u_j} u_j), u_m - u^\dagger \right\rangle \right| \\ &\leq \sum_{j=m}^{\ell-1} \left| \left\langle \alpha_j \mathcal{F}'(u_j)^*(\mathcal{F}(u_j) - v), u_m - u^\dagger \right\rangle \right| + \sum_{j=m}^{\ell-1} \left| \left\langle \beta_j \Delta_{u_j} u_j, u_m - u^\dagger \right\rangle \right| \\ &\leq \zeta_1 \sum_{j=m}^{\ell-1} \left| \left\langle \mathcal{F}(u_j) - v, \mathcal{F}'(u_j)(u_m - u^\dagger) \right\rangle \right| + \sum_{j=m}^{\ell-1} \beta_j \left| \left\langle \Delta_{u_j} u_j, u_m - u^\dagger \right\rangle \right| \\ &\leq \zeta_1 \sum_{j=m}^{\ell-1} \|\mathcal{F}(u_j) - v\| \|\mathcal{F}'(u_j)(u_m - u^\dagger)\| + \sum_{j=m}^{\ell-1} \beta_j \|\Delta_{u_j} u_j\| \|u_m - u^\dagger\|. \end{aligned}$$

Using (A3) of Assumption 2.3, it can be easily obtain that

$$\begin{aligned} (26) \quad \|\mathcal{F}'(u_j)(u_m - u^\dagger)\| &\leq \|\mathcal{F}'(u_j)(u_j - u^\dagger)\| + \|\mathcal{F}'(u_j)(u_m - u_j)\| \\ &\leq (1 + \eta) (\|\mathcal{F}(u_j) - v\| + \|\mathcal{F}(u_m) - \mathcal{F}(u_j)\|) \\ &\leq (1 + \eta) (2\|\mathcal{F}(u_j) - v\| + \|\mathcal{F}(u_m) - v\|). \end{aligned}$$

Employing (20), (26), and the inequality $\beta_j \|\Delta_{u_j} u_j\| \leq \nu_0 \|\mathcal{F}(u_j) - v\|^2$, from (10), and observing that $u_k \in \mathcal{B}_\varphi(u^\dagger)$ for all $k \geq 0$, the preceding inequality can be equivalently transformed as

$$\begin{aligned} |\langle g_m - g_\ell, g_m \rangle| &\leq 3\zeta_1(1 + \eta) \sum_{j=m}^{\ell-1} \|\mathcal{F}(u_j) - v\|^2 + \varphi \nu_0 \sum_{j=m}^{\ell-1} \|\mathcal{F}(u_j) - v\|^2 \\ (27) \quad &\leq \left(3\zeta_1(1 + \eta) + \varphi \nu_0 \right) \sum_{j=m}^{\ell-1} \|\mathcal{F}(u_j) - v\|^2. \end{aligned}$$

Applying the same reasoning to $|\langle g_k - g_m, g_m \rangle|$, we can obtain

$$(28) \quad |\langle g_k - g_m, g_m \rangle| \leq \left(3\zeta_1(1 + \eta) + \varphi \nu_0 \right) \sum_{j=k}^{m-1} \|\mathcal{F}(u_j) - v\|^2.$$

Now, using (27) and (28) we deduce that $|\langle g_m - g_\ell, g_m \rangle|$ and $|\langle g_k - g_m, g_m \rangle|$ converge to zero as $k \rightarrow \infty$, by virtue of (19). So, from (24) and (25), we have

$$\begin{aligned}\lim_{k \rightarrow \infty} \|g_l - g_m\|^2 &= 2 \lim_{k \rightarrow \infty} \langle g_m - g_l, g_m \rangle = 0, \\ \lim_{k \rightarrow \infty} \|g_m - g_k\|^2 &= 2 \lim_{k \rightarrow \infty} \langle g_k - g_m, g_m \rangle = 0.\end{aligned}$$

It is straightforward from (21), (22), and (23) that the sequence $\{g_k\}_{k \geq 0}$ is Cauchy. Therefore, $\{u_k\}_{k \geq 0}$ likewise forms a Cauchy sequence and converges to a limit u^* . Given that $F(u_k) - v$ vanishes as $k \rightarrow \infty$, the limit satisfies (1), suggesting $u^* = u^\dagger$. Thus, the iterates generated by exact data variant of E-IRMGL+ Ψ (3) converge to the true solution of (1). \square

3.3. Stability analysis. This subsection, investigates the stability of the E-IRMGL+ Ψ approach in the presence of multiple repeated measurement data. We require the following regularity condition on the family of reconstructors Ψ_θ .

Assumption 3.5. *Let $\hat{v}^{(m)} := \frac{1}{m} \sum_{i=1}^m v_i$ denote the empirical mean, and let $\theta = \theta(m, \hat{v}^{(m)})$ be fixed. We assume that the reconstruction operator $\Psi_\theta : \mathcal{V} \rightarrow \mathcal{U}$ is mean-square continuous, i.e., for sequences $m_r \rightarrow m$ and $\hat{v}^{(m_r)} \rightarrow \hat{v}^{(m)}$ as $r \rightarrow \infty$, and $\theta_r := \theta(m_r, \hat{v}^{(m_r)})$, it holds that*

$$\mathbb{E}[\theta_r] \rightarrow \mathbb{E}[\theta] \quad \text{and} \quad \mathbb{E}[\|\Psi_{\theta_r}(\hat{v}^{(m_r)}) - \Psi_\theta(\hat{v}^{(m)})\|^2] \rightarrow 0 \quad \text{as } r \rightarrow \infty.$$

It is crucial to emphasize that the aforementioned assumption is the stochastic variant of [10, Hypothesis 3.2], and we are working on $\hat{v}^{(m)}$ instead of noisy data v^δ . It should be noted that a wide class of reconstructors can satisfy this weak assumption. We verify Assumption 3.5 on a standard reconstructor given below and clarify the role and admissible dependence of the parameter $\theta = \theta(m, \hat{v}^{(m)})$.

Tikhonov reconstructors. Define the Tikhonov functional

$$\mathcal{J}_\theta(u; v) := \frac{1}{2} (\|\mathcal{F}(u) - v\|^2 + \theta\|u\|^2), \quad v \in \mathcal{V},$$

where $\theta \in (0, \infty)$. Suppose there exist a radius $\varphi > 0$ and a constant $c_\theta > 0$ such that for every $u \in \mathcal{B}_\varphi(u^\dagger)$ the Hessian of \mathcal{J}_θ at u satisfies the uniform coercivity bound

$$\langle (\mathcal{F}'(u)^* \mathcal{F}'(u) + \theta I)w, w \rangle \geq c_\theta \|w\|^2 \quad \text{for all } w \in \mathcal{U}.$$

Then for every v sufficiently close to $\mathcal{F}(u^\dagger)$ the minimizer

$$\Psi_\theta(v) := \arg \min_{u \in \mathcal{B}_\varphi(u^\dagger)} \mathcal{J}_\theta(u; v)$$

exists and is unique. Let $\theta = \theta(m, \hat{v}^{(m)})$ denotes the regularization parameter determined via the statistical version of the discrepancy principle [20, equation (4.57)], then the parameter sequence is stable in expectation, in the sense that

$$\mathbb{E}[\theta_r] \rightarrow \mathbb{E}[\theta] \quad \text{as } r \rightarrow \infty.$$

Moreover the map $(v, \theta) \mapsto \Psi_\theta(v)$ is joint locally Lipschitz, i.e., there exists a constant $L_v, L_\theta > 0$ (depending on θ and the local behavior of \mathcal{F}) such that

$$\|\Psi_{\theta_r}(\hat{v}^{(m_r)}) - \Psi_\theta(\hat{v}^{(m)})\| \leq L_v \|\hat{v}^{(m_r)} - \hat{v}^{(m)}\| + L_\theta |\theta_r - \theta|$$

for all $\hat{v}^{(m_r)}, \hat{v}^{(m)}$ in a small neighborhood of $\mathcal{F}(u^\dagger)$. Consequently, we have the desired result. In the linear setting, the verification of Assumption 3.5 becomes significantly simpler. One may follow the argument outlined in [10, Example A.6], which provides a direct and concise proof tailored to the linear case.

Before proceeding to the main stability result, we note that the regularization term of E-IRMGL+ Ψ method depends explicitly on the empirical mean $\hat{v}^{(m)}$. This dependence prevents a direct application of standard analytical techniques and making it highly nonstandard. To address this difficulty, we rely on a lemma, originally established in [5, 10], which is central to our stability analysis.

Lemma 3.6. *For the sequence of iterates $\{u_k^{(m)}\}_{k \geq 0}$ generated by Algorithm 1 and the sequence of iterates $\{u_k\}_{k \geq 0}$ generated by its exact data counterpart, the following holds*

$$\|\Delta_{u_k^{(m)}} u_k - \Delta_{u_k} u_k\| \leq \mathcal{H}_0 \|u_k\| \|u_k^{(m)} - u_k\|,$$

where

$$\mathcal{H}_0 = 2L_h \left(\max_{a,b} g(a,b) \sqrt{D_N} + \max_a \max_b g(a,b) \right),$$

with $g(a,b)$ as in (6), L_h is the Lipschitz constant of the function h_u and D_N denotes the maximum degree of any node in \mathcal{S} .

We now show that Lemma 3.6, together with Assumption 3.5, ensures the stability linking Algorithm 1 with its exact counterpart. Since the iterates $u_k^{(m)}$ of Algorithm 1 are random variables, the analysis is carried out in a stochastic framework.

Lemma 3.7. *Let Assumptions 2.3, 2.5, and 3.5 be satisfied. Then, for every fixed integer $k \geq 0$, the iterates $u_k^{(m)}$ produced by Algorithm 1 converge in mean square to the corresponding exact-data iterates u_k , i.e.,*

$$\lim_{m \rightarrow \infty} \mathbb{E} \left[\|u_k^{(m)} - u_k\|^2 \right] = 0.$$

Proof. We proceed by induction. For $k = 0$, since $u_0^{(m)} = \Psi_\theta(\hat{v}^{(m)})$ and $u_0 = \Psi(v)$, the result follows immediately from Assumption 3.5, which ensures

$$\mathbb{E} \left[\|u_0^{(m)} - u_0\|^2 \right] \rightarrow 0 \quad \text{as } m \rightarrow \infty.$$

Let us now assume that the assertion is true for all $0 \leq j \leq k$, that is, as m approaches ∞ , $\mathbb{E}[\|u_j^{(m)} - u_j\|^2] \rightarrow 0$. Our goal is to demonstrate that it also applies to $j = k + 1$. To do so, observe from (3) that

$$(29) \quad \begin{aligned} u_{k+1}^{(m)} - u_{k+1} &= \left(u_k^{(m)} - u_k \right) - \left(\beta_k^{(m)} \Delta_{u_k^{(m)}} u_k^{(m)} - \beta_k \Delta_{u_k} u_k \right) \\ &\quad - \left(\alpha_k^{(m)} \mathcal{F}'(u_k^{(m)})^* (\mathcal{F}(u_k^{(m)}) - \hat{v}^{(m)}) - \alpha_k \mathcal{F}'(u_k)^* (\mathcal{F}(u_k) - v) \right). \end{aligned}$$

Taking the squared norm and subsequently the expectation yields

$$(30) \quad \begin{aligned} \mathbb{E} \left[\|u_{k+1}^{(m)} - u_{k+1}\|^2 \right] &\leq 3 \left(\mathbb{E} \left[\|u_k^{(m)} - u_k\|^2 \right] \right. \\ &\quad \left. + \mathbb{E} \left[\|\alpha_k^{(m)} \mathcal{F}'(u_k^{(m)})^* (\mathcal{F}(u_k^{(m)}) - \hat{v}^{(m)}) - \alpha_k \mathcal{F}'(u_k)^* (\mathcal{F}(u_k) - v)\|^2 \right] \right. \\ &\quad \left. + \mathbb{E} \left[\|\beta_k^{(m)} \Delta_{u_k^{(m)}} u_k^{(m)} - \beta_k \Delta_{u_k} u_k\|^2 \right] \right) := 3(I + II + III), \end{aligned}$$

where we have employed the inequality $(a_1 + a_2 + a_3)^2 \leq 3(a_1^2 + a_2^2 + a_3^2)$ for $a_1, a_2, a_3 \in \mathbb{R}$. Note that $I \rightarrow 0$ by induction argument. We now turn to the estimate of II . For this, let

$$\mathcal{A}_m := \mathcal{F}'(u_k^{(m)})^* (\mathcal{F}(u_k^{(m)}) - \hat{v}^{(m)}), \quad \mathcal{A} := \mathcal{F}'(u_k)^* (\mathcal{F}(u_k) - v),$$

and denote $\alpha_m := \alpha_k^{(m)}$, $\alpha := \alpha_k$. Then

$$\alpha_m \mathcal{A}_m - \alpha \mathcal{A} = \alpha_m (\mathcal{A}_m - \mathcal{A}) + (\alpha_m - \alpha) \mathcal{A}.$$

By the standard inequality $\|x + y\|^2 \leq 2\|x\|^2 + 2\|y\|^2$, we obtain

$$(31) \quad \mathbb{E} [\|\alpha_m \mathcal{A}_m - \alpha \mathcal{A}\|^2] \leq 2\mathbb{E} [\alpha_m^2 \|\mathcal{A}_m - \mathcal{A}\|^2] + 2\mathbb{E} [(\alpha_m - \alpha)^2 \|\mathcal{A}\|^2].$$

We now expand $\mathcal{A}_m - \mathcal{A}$ as

$$\begin{aligned} \mathcal{A}_m - \mathcal{A} &= (\mathcal{F}'(u_k^{(m)})^* - \mathcal{F}'(u_k)^*) (\mathcal{F}(u_k) - v) \\ &\quad + [\mathcal{F}'(u_k^{(m)})^* (\mathcal{F}(u_k^{(m)}) - \hat{v}^{(m)}) - \mathcal{F}'(u_k^{(m)})^* (\mathcal{F}(u_k) - v)]. \end{aligned}$$

By combining the operator norm inequality with the triangle inequality, and invoking both the uniform boundedness and the Lipschitz continuity of \mathcal{F}' (cf. (A2) and (A4) of Assumption 2.3), we obtain

$$\|\mathcal{A}_m - \mathcal{A}\| \leq L\|u_k^{(m)} - u_k\| \|\mathcal{F}(u_k) - v\| + B\|\mathcal{F}(u_k^{(m)}) - \mathcal{F}(u_k) - \hat{v}^{(m)} + v\|.$$

Furthermore, (A2) and (A3) of Assumption 2.3 ensures that

$$\|\mathcal{F}(u_k) - v\| \leq \frac{1}{1-\eta} \|\mathcal{F}'(u^\dagger)(u_k - u^\dagger)\| \leq \frac{B}{1-\eta} \|u_k - u^\dagger\|.$$

Since Theorem theorem 3.4 guarantees that the sequence u_k remains bounded, it follows that $\|\mathcal{F}(u_k) - v\|$ is also bounded. Taking squared norms and expectations then yields

$$\begin{aligned} \mathbb{E} [\|\mathcal{A}_m - \mathcal{A}\|^2] &\leq 2 \left(L^2 \|\mathcal{F}(u_k) - v\|^2 \mathbb{E} [\|u_k^{(m)} - u_k\|^2] \right. \\ &\quad \left. + B^2 \mathbb{E} [\|\mathcal{F}(u_k^{(m)}) - \mathcal{F}(u_k) - \hat{v}^{(m)} + v\|^2] \right) \\ &\leq 2 \left(L^2 \|\mathcal{F}(u_k) - v\|^2 \mathbb{E} [\|u_k^{(m)} - u_k\|^2] \right. \\ &\quad \left. + 2B^2 \left(\mathbb{E} [\|\mathcal{F}(u_k^{(m)}) - \mathcal{F}(u_k)\|^2] + \mathbb{E} [\|\hat{v}^{(m)} - v\|^2] \right) \right) \\ &\leq 2 \left(L^2 \|\mathcal{F}(u_k) - v\|^2 + \frac{2B^4}{(1-\eta)^2} \right) \mathbb{E} [\|u_k^{(m)} - u_k\|^2] + 4B^2 \frac{\sigma^2}{m}. \end{aligned}$$

By assumption, we have $\mathbb{E} [\|u_k^{(m)} - u_k\|^2] \rightarrow 0$ and $\frac{\sigma^2}{m} \rightarrow 0$ as $m \rightarrow \infty$. Moreover, since $\alpha_m \leq \zeta_1$ by definition, it follows that

$$(32) \quad \mathbb{E} [\alpha_m^2 \|\mathcal{A}_m - \mathcal{A}\|^2] \leq \zeta_1^2 \mathbb{E} [\|\mathcal{A}_m - \mathcal{A}\|^2] \rightarrow 0.$$

Next, we establish that $\alpha_m \rightarrow \alpha$ in $\mathcal{L}^2(\Omega, \mathcal{U})$, which directly implies

$$\mathbb{E} [(\alpha_m - \alpha)^2 \|\mathcal{A}\|^2] = \|\mathcal{A}\|^2 \mathbb{E} [(\alpha_m - \alpha)^2] \rightarrow 0.$$

Since $u_k^{(m)} \rightarrow u_k$ and $\hat{v}^{(m)} \rightarrow v$ as $m \rightarrow \infty$ in mean-square, Chebyshev's inequality gives, for any $\varepsilon > 0$,

$$\mathbb{P} (\|u_k^{(m)} - u_k\| > \varepsilon) \leq \frac{\mathbb{E} [\|u_k^{(m)} - u_k\|^2]}{\varepsilon^2} \rightarrow 0,$$

and similarly for $\hat{v}^{(m)}$. Hence $(u_k^{(m)}, \hat{v}^{(m)}) \rightarrow (u_k, v)$ in probability. Now, define

$$\phi(u, v) := \frac{\zeta_0 \|\mathcal{F}(u) - v\|}{\|\mathcal{F}'(u)^* (\mathcal{F}(u) - v)\|},$$

with the understanding that ϕ is considered only in a neighborhood of (u_k, v) where the denominator is nonzero. By (A4) of Assumption 2.3, the map $(u, v) \mapsto \phi(u, v)$ is continuous at (u_k, v) because $\|\mathcal{F}'(u_k)^* (\mathcal{F}(u_k) - v)\| = \|\mathcal{A}\| \neq 0$ implies the denominator stays bounded away from zero in a small neighborhood. So, the function

$$\psi(u, v) := \min \{\phi(u, v), \zeta_1\}$$

is therefore also continuous at (u_k, v) . Since $\alpha_m = \psi(u_k^{(m)}, \hat{v}^{(m)})$ and $\alpha = \psi(u_k, v)$, the continuous mapping theorem yields $\alpha_m \xrightarrow{P} \alpha$ (convergence in probability). By definition $0 \leq \alpha_m \leq \zeta_1$ and $0 \leq \alpha \leq \zeta_1$, hence

$$0 \leq Z_m := |\alpha_m - \alpha|^2 \leq 4\zeta_1^2 < \infty \quad \text{a.s.}$$

We already have $Z_m \xrightarrow{P} 0$. We claim $\mathbb{E}[Z_m] \rightarrow 0$. To prove this, assume for contradiction that $\mathbb{E}[Z_m] \not\rightarrow 0$. Then there exists $\varepsilon > 0$ and a subsequence (Z_{m_j}) with $\mathbb{E}[Z_{m_j}] \geq \varepsilon$ for all j . Since $Z_{m_j} \rightarrow 0$ in probability, by the subsequence principle there exists a further sub-subsequence $(Z_{m_{j_\ell}})$ that converges to 0 almost surely. Because $0 \leq Z_{m_{j_\ell}} \leq 4\zeta_1^2$ and $4\zeta_1^2$ is integrable, the dominated convergence theorem implies that $\mathbb{E}[Z_{m_{j_\ell}}] \rightarrow 0$, which contradicts $\mathbb{E}[Z_{m_j}] \geq \varepsilon$. Thus no such subsequence exists and we must have $\mathbb{E}[Z_m] \rightarrow 0$. Equivalently, $\mathbb{E}[(\alpha_m - \alpha)^2] \rightarrow 0$, i.e. $\alpha_m \rightarrow \alpha$ in $\mathcal{L}^2(\Omega, \mathcal{U})$. Therefore, we obtain

$$(33) \quad \mathbb{E}[(\alpha_m - \alpha)^2 \|\mathcal{A}\|^2] = \|\mathcal{A}\|^2 \mathbb{E}[(\alpha_m - \alpha)^2] \rightarrow 0.$$

Using (32) and (33) in (31), we obtain

$$(34) \quad \Pi := \mathbb{E}[\|\alpha_m \mathcal{A}_m - \alpha \mathcal{A}\|^2] \rightarrow 0 \quad \text{as } m \rightarrow \infty.$$

Similarly, for the III term, assuming that $\|\Delta_{u_k^{(m)}} u_k^{(m)}\| \neq 0$ and using the definition of $\beta_k^{(m)}$ in (10), it can be shown that $\beta_k^{(m)} \rightarrow \beta_k$ in $\mathcal{L}^2(\Omega, \mathcal{U})$, in complete analogy with the convergence $\alpha_k^{(m)} \rightarrow \alpha_k$ in $\mathcal{L}^2(\Omega, \mathcal{U})$. As a consequence, we obtain

$$(35) \quad \begin{aligned} \text{III} &\leq 2\mathbb{E}\left[\|\beta_k^{(m)} \Delta_{u_k^{(m)}}(u_k^{(m)} - u_k)\|^2\right] + 2\mathbb{E}\left[\|(\beta_k^{(m)} \Delta_{u_k^{(m)}} - \beta_k \Delta_{u_k})u_k\|^2\right] \\ &\leq 2\nu_2^2 \mathbb{E}\left[\|\Delta_{u_k^{(m)}}(u_k^{(m)} - u_k)\|^2\right] + 4\mathbb{E}\left[\|(\beta_k^{(m)} - \beta_k) \Delta_{u_k^{(m)}} u_k\|^2\right] \\ &\quad + 4\nu_2^2 \mathbb{E}\left[\|(\Delta_{u_k^{(m)}} - \Delta_{u_k}) u_k\|^2\right] \rightarrow 0 \quad \text{as } m \rightarrow \infty. \end{aligned}$$

Here, the last convergence follows from the facts that $\mathbb{E}[|\beta_k^{(m)} - \beta_k|^2] \rightarrow 0$, the induction hypothesis, and Lemma 3.6. Combining (34), (35) with (30) and the induction hypothesis, we conclude that $\mathbb{E}[\|u_{k+1}^{(m)} - u_{k+1}\|^2] \rightarrow 0$ as $m \rightarrow \infty$. This completes the induction step, and therefore the proof. \square

3.4. Convergence for noisy data. In this subsection, we establish the regularization property of the E-IRMGL+ Ψ method introduced in Algorithm 1. Specifically, we provide a detailed convergence analysis in the theorem stated below.

Theorem 3.8. *Assuming all the convictions of Lemma 3.7 are true and k_m is the stopping index for Algorithm 1 as specified in rule 2, then a solution u^\dagger of (1) exists such that*

$$\lim_{m \rightarrow \infty} \mathbb{E}\left[\|u_{k_m}^{(m)} - u^\dagger\|^2\right] = 0.$$

Proof. Consider a sequence $\{m_r\}$ with $m_r \rightarrow \infty$ and $\frac{\tau_{m_r}}{\sqrt{m_r}} \rightarrow 0$ as $r \rightarrow \infty$, and let $\hat{v}^{(m_r)}$ be the associated empirical mean of the measurement data. For each $(m_r, \hat{v}^{(m_r)})$, the stopping index given by rule 2 is denoted by $k_r := k_{m_r}$. Let u^\dagger be the solution of (1) from Theorem 3.4, satisfying $\|u_k - u^\dagger\| \rightarrow 0$ as $k \rightarrow \infty$, where $\{u_k\}_{k \geq 0}$ are the iterates generated by the exact data counterpart of Algorithm 1. In order to determine the intended outcome, we will look at two scenarios.

Case-I: Suppose that for some finite integer $K > 0$, the sequence $k_r \rightarrow K$ as $r \rightarrow \infty$. Then, for sufficiently large $r \geq 0$, we may set $k_r = K$. Consequently, by the definition of k_r , it follows that

$$\|\mathcal{F}(u_K^{(m_r)}) - \hat{v}^{(m_r)}\| \leq \frac{\tau_{m_r}}{\sqrt{m_r}} z_{m_r}.$$

Further, we have

$$\begin{aligned}\|\mathcal{F}(u_K) - v\| &\leq \|\mathcal{F}(u_K) - \mathcal{F}(u_K^{(m_r)})\| + \|\mathcal{F}(u_K^{(m_r)}) - \hat{v}^{(m_r)}\| + \|\hat{v}^{(m_r)} - v\| \\ &\leq \|\mathcal{F}(u_K) - \mathcal{F}(u_K^{(m_r)})\| + \frac{\tau_{m_r}}{\sqrt{m_r}} z_{m_r} + \|\hat{v}^{(m_r)} - v\|.\end{aligned}$$

Taking the expectation and considering the assertion

$$\mathbb{E}[z_m] \leq \mathbb{E}[z_m^2]^{1/2} \leq \sigma \quad \text{and} \quad \mathbb{E}[\|v - \hat{v}^{(m_r)}\|] \leq \mathbb{E}[\|v - \hat{v}^{(m_r)}\|^2]^{1/2} = \frac{\sigma}{\sqrt{m_r}},$$

we deduce

$$\|\mathcal{F}(u_K) - v\| \leq \mathbb{E} \left[\|\mathcal{F}(u_K) - \mathcal{F}(u_K^{(m_r)})\| \right] + \frac{\tau_{m_r}}{\sqrt{m_r}} \sigma + \frac{\sigma}{\sqrt{m_r}}.$$

Taking the limit as $r \rightarrow \infty$ and applying Lemma 3.7 along with the continuity of \mathcal{F} , we obtain $\mathcal{F}(u_K) = v$. Then, using Theorem 3.4, it can be shown that $u_{k_r} = u_K = u^\dagger$. As a result, we deduce that

$$\mathbb{E} \left[\|u_{k_r}^{(m_r)} - u_{k_r}\|^2 \right] = \mathbb{E} \left[\|u_{k_r}^{(m_r)} - u^\dagger\|^2 \right] \rightarrow 0 \quad \text{as } r \rightarrow \infty.$$

Case-II: Assume that there exists a subsequence $\{m_r\}$ with $m_r \rightarrow \infty$ such that the corresponding stopping indices satisfy $k_r := k_{m_r} \rightarrow \infty$ as $r \rightarrow \infty$. Let k be a fixed but sufficiently large integer. From Lemma 3.3, there exists $\varepsilon > 0$ such that $\|u_k - u^\dagger\| \leq \frac{\sqrt{\varepsilon}}{2\sqrt{2}}$. Moreover, by Lemma 3.7, for this fixed k there exists $n = n(k, \varepsilon)$ such that

$$\mathbb{E} \left[\|u_k^{(m)} - u_k\|^2 \right]^{1/2} \leq \frac{\sqrt{\varepsilon}}{2\sqrt{2}}, \quad \forall m > n(k, \varepsilon).$$

Let $\chi_{\Gamma_{m_r}}$ denotes the characteristic function of Γ_{m_r} . Then, as in [31, Theorem 3.10], we have

$$(36) \quad \mathbb{E} \left[\|u_{k_r}^{(m_r)} - u^\dagger\|^2 \right] = \underbrace{\mathbb{E} \left[\|u_{k_r}^{(m_r)} - u^\dagger\|^2 \chi_{\Gamma_{m_r}} \right]}_{\text{I}} + \underbrace{\mathbb{E} \left[\|u_{k_r}^{(m_r)} - u^\dagger\|^2 \chi_{\Gamma_{m_r}^c} \right]}_{\text{II}}.$$

We now proceed to bound both terms in (36). For the first term, observe that for large enough r such that $k_r > k$, Lemma 3.1 ensures that, on the event Γ_{m_r} , the iterates exhibit monotonicity in expectation. That is,

$$\mathbb{E} \left[\|u_{k_r}^{(m)} - u^\dagger\|^2 \right]^{1/2} \leq \mathbb{E} \left[\|u_k^{(m)} - u^\dagger\|^2 \right]^{1/2}.$$

Finally, by the triangle inequality inside the expectation norm, we obtain

$$\mathbb{E} \left[\|u_k^{(m)} - u^\dagger\|^2 \right]^{1/2} \leq \mathbb{E} \left[\|u_k^{(m)} - u_k\|^2 \right]^{1/2} + \|u_k - u^\dagger\| \leq \sqrt{\frac{\varepsilon}{2}}.$$

Thus,

$$\text{I} := \mathbb{E} \left[\|u_{k_r}^{(m_r)} - u^\dagger\|^2 \chi_{\Gamma_{m_r}} \right] \leq \mathbb{E} \left[\|u_{k_r}^{(m_r)} - u^\dagger\|^2 \right] \leq \frac{\varepsilon}{2}.$$

To bound the second term, observe that $\lim_{r \rightarrow \infty} \mathbb{P}(\Gamma_{m_r}^c) = 0$. So it suffices to bound $\mathbb{E} \left[\|u_{k_r}^{(m_r)} - u^\dagger\|^2 \right]$ with a constant, independent of m_r . Since

$$\mathbb{E} \left[\|u_{k_r}^{(m_r)} - u^\dagger\|^2 \right]^{1/2} \leq \mathbb{E} \left[\|u_{k_r}^{(m_r)} - u_{k_r}\|^2 \right]^{1/2} + \|u_k - u^\dagger\|.$$

It follows from (18) that the sequence $\{\|u_k - u^\dagger\|\}$ is bounded by $\|u_0 - u^\dagger\|$. Moreover, if r is sufficiently large then from Lemma 3.7, $\mathbb{E} \left[\|u_{k_r}^{(m_r)} - u_{k_r}\|^2 \right]^{1/2}$ is also bounded by some constant $M > 0$. Hence

$$\text{II} := \mathbb{E} \left[\|u_{k_r}^{(m_r)} - u^\dagger\|^2 \chi_{\Gamma_{m_r}^c} \right] \leq M \mathbb{P}(\Gamma_{m_r}^c) \leq \frac{\varepsilon}{2}.$$

Now, with the bounds of I and II in (36), we have

$$\mathbb{E} \left[\|u_{k_r}^{(m_r)} - u^\dagger\|^2 \right] = \text{I} + \text{II} \leq \frac{\varepsilon}{2} + \frac{\varepsilon}{2} = \varepsilon$$

which completes the proof. \square

4. CONVERGENCE ANALYSIS UNDER HEURISTIC RULE

In this section, we analyze the regularization properties of **E-IRMGL+ Ψ** (3) when terminated according to rule 1. Throughout this analysis, we assume that Assumption 2.6 holds. To facilitate the subsequent discussion, we present the scheme in the form of Algorithm 2.

Algorithm 2 **E-IRMGL+ Ψ** with heuristic principle

1: **Input:** Operator \mathcal{F} , measurements v_1, v_2, \dots, v_m , initial reconstructor Ψ_θ , parameters θ, λ, R , and $\varrho \geq 1$.

2: **Set:** $\hat{v}^{(m)} := \frac{1}{m} \sum_{i=1}^m v_i$ and $z_m := \sqrt{\frac{1}{m-1} \sum_{i=1}^m \|v_i - \hat{v}^{(m)}\|^2}$.

3: **Initialize:** $u_0^{(m)} := \Psi_\theta(\hat{v}^{(m)})$.

4: **Iteration:** For $k = 0, 1, \dots, k_\infty$ (with $u_k^{(m)} \in \mathcal{D}(\mathcal{F})$), compute

$$u_{k+1}^{(m)} := u_k^{(m)} - \alpha_k^{(m)} \mathcal{F}'(u_k^{(m)})^* \left(\mathcal{F}(u_k^{(m)}) - \hat{v}^{(m)} \right) - \beta_k^{(m)} \Delta_{u_k^{(m)}} u_k^{(m)},$$

where $\alpha_k^{(m)}$ and $\beta_k^{(m)}$ are given by (9) and (10), and $\Delta_{u_k^{(m)}}$ is defined in Section 2.1.

5: **Stopping rule:** Determine the index

$$k_m^* \in \arg \min \left\{ \Omega(k, \hat{v}^{(m)}) : 0 \leq k \leq k_\infty \right\}, \quad \text{where}$$

$$\Omega(k, \hat{v}^{(m)}) := (k + \varrho) \| \mathcal{F}(u_k^{(m)}) - \hat{v}^{(m)} \|^2.$$

6: **Output:** $u_{k_m^*}^{(m)}$.

Remark 4.1. Rule 1 is straightforward to implement. During iteration, we record $\Omega(k, \hat{v}^{(m)})$ against k and, after sufficient iterations, select k_m^* that minimizes it. Since the iterative regularization methods for nonlinear problems may exhibits only local convergence [24], so the maximum iteration count must be chosen large enough to avoid mistaking a local for the global minimum. The rule requires a fixed constant ϱ , introduced in [29] for the augmented Lagrangian method, where a similar stopping strategy was used. Choosing ϱ sufficiently large ensures an accurate solution and prevents k_m^* from being underestimated. Previous numerical and analytical studies [29, 45, 49] indicate that the lower bound of ϱ depends on the regularization method and for the Landweber iteration $\varrho \geq 1$ is essential. In our method we also require that $\varrho \geq 1$, which can be seen later in Lemma 4.2.

4.1. Preliminary analysis. We first establish that

$$(37) \quad \Omega(k_m^*, \hat{v}^{(m)}) \rightarrow 0 \quad \text{as } m \rightarrow \infty,$$

where $\Omega(\cdot, \cdot)$ is defined in rule 1. To this end, we introduce an auxiliary index \hat{k}_m , determined by the stopping rule as the smallest integer satisfying

$$(38) \quad \left\| \mathcal{F}(u_{\hat{k}_m}^{(m)}) - \hat{v}^{(m)} \right\|^2 + \frac{\mathcal{M}}{(\hat{k}_m + \varrho)^2} \leq \frac{\tau_m^2}{m} z_m^2,$$

where $\tau_m \geq 1$ may depend on m , and $\mathcal{M} = \frac{3\mathcal{H}\varphi^2}{2(1+\eta)\zeta_1}$. It is worth noting that the stopping rule in (38) is a modification of rule 2 through the inclusion of the additional term $\frac{\mathcal{M}}{(k+\varrho)^2}$. The presence of this term ensures that $\hat{k}_m \rightarrow \infty$ as $m \rightarrow \infty$, which is a crucial ingredient in the proof of (37).

Lemma 4.2. *Suppose that $\mathcal{C} > 0$ as defined in (11) and all the assumptions of Lemma 3.1 satisfies, then the following hold.*

- (i.) $u_k^{(m)} \in \mathcal{B}_{3\varphi}(u_0)$ for all $0 \leq k \leq \hat{k}_m$, where \hat{k}_m is the stopping index as in (38).
- (ii.) \hat{k}_m is a finite integer and $\hat{k}_m \rightarrow \infty$ as $m \rightarrow \infty$.

Proof. Following the same procedure of Lemma 3.1, we have

$$(39) \quad \|g_{k+1}^{(m)}\|^2 - \|g_k^{(m)}\|^2 = \|h_k^{(m)}\|^2 - 2\langle g_k^{(m)}, h_k^{(m)} \rangle$$

along with the estimates

$$(40) \quad -\langle g_k^{(m)}, h_k^{(m)} \rangle \leq -(1-\eta)\alpha_k^{(m)} \|\mathcal{F}(u_k^{(m)}) - \hat{v}^{(m)}\|^2 + \varphi\nu_0 \|\mathcal{F}(u_k^{(m)}) - \hat{v}^{(m)}\|^2 + (1+\eta)\alpha_k^{(m)} \|v - \hat{v}^{(m)}\| \|\mathcal{F}(u_k^{(m)}) - \hat{v}^{(m)}\|$$

$$(41) \quad \|h_k^{(m)}\|^2 \leq 2(\zeta_0^2 + \nu_0\nu_1) \|\mathcal{F}(u_k^{(m)}) - \hat{v}^{(m)}\|^2.$$

Now, utilizing the property of the space Γ_m and according to the definition of \hat{k}_m , for $k < \hat{k}_m$ we have

$$\|v - \hat{v}^{(m)}\| \leq \frac{\tau_m}{\mathcal{H}\sqrt{m}} z_m \leq \frac{1}{\mathcal{H}} \left(\|\mathcal{F}(u_k^{(m)}) - \hat{v}^{(m)}\|^2 + \frac{\mathcal{M}}{(k+\varrho)^2} \right)^{1/2}$$

and by the inequality $2a_1a_2 \leq a_1^2 + a_2^2$ for $a_1, a_2 \in \mathbb{R}$, we further have

$$(42) \quad \|v - \hat{v}^{(m)}\| \|\mathcal{F}(u_k^{(m)}) - \hat{v}^{(m)}\| \leq \frac{1}{\mathcal{H}} \left(\|\mathcal{F}(u_k^{(m)}) - \hat{v}^{(m)}\|^2 + \frac{\mathcal{M}}{2(k+\varrho)^2} \right).$$

Using (40), (41) and (42) in (39), we get

$$\|g_{k+1}^{(m)}\|^2 - \|g_k^{(m)}\|^2 \leq -2\mathcal{C} \|\mathcal{F}(u_k^{(m)}) - \hat{v}^{(m)}\|^2 + \frac{\mathcal{M}(1+\eta)\zeta_1}{\mathcal{H}(k+\varrho)^2}.$$

Now, taking the sum from $n = 0$ to $n = k$ on both side, we further obtain

$$(43) \quad \|g_{k+1}^{(m)}\|^2 + 2\mathcal{C} \sum_{n=0}^k \|\mathcal{F}(u_n^{(m)}) - \hat{v}^{(m)}\|^2 \leq \|g_0^{(m)}\|^2 + \frac{\mathcal{M}(1+\eta)\zeta_1}{\mathcal{H}} \sum_{n=0}^k \frac{1}{(n+\varrho)^2}.$$

Note that $\varrho \geq 1$, $\mathcal{M} = \frac{3\mathcal{H}\varphi^2}{2(1+\eta)\zeta_1}$ and since $\sum_{n=0}^k \frac{1}{(n+\varrho)^2} \leq \sum_{n=0}^{\infty} \frac{1}{(n+\varrho)^2} = \frac{\pi^2}{6} < 2$, it yields

$$\|u_{k+1}^{(m)} - u^\dagger\|^2 \leq \|u_0^{(m)} - u^\dagger\|^2 + 3\varphi^2 \leq 4\varphi^2.$$

Hence, we have $u_{k+1}^{(m)} \in \mathcal{B}_{2\varphi}(u^\dagger)$. Since $\|u_0 - u^\dagger\| \leq \varphi$, we therefore have $u_{k+1}^{(m)} \in \mathcal{B}_{3\varphi}(u_0)$. To prove (ii), let us suppose a contrary, that is \hat{k}_m is infinite. Then from (43), we have

$$(44) \quad 2\mathcal{C} \sum_{n=0}^k \|\mathcal{F}(u_n^{(m)}) - \hat{v}^{(m)}\|^2 \leq 4\varphi^2 \quad \forall k \geq 0.$$

Additionally, the definition of \hat{k}_m tells us that for every integer $k \geq 0$ we have

$$\frac{\tau_m^2}{m} z_m^2 - \frac{\mathcal{M}}{(k+\varrho)^2} < \|\mathcal{F}(u_k^{(m)}) - \hat{v}^{(m)}\|^2.$$

Summing up the above inequality from $n = 0$ to $n = k < \hat{k}_m$ and then using (44),

$$\frac{\tau_m^2 z_m^2}{m} (k+1) \leq \mathcal{M} \sum_{n=0}^k \frac{1}{(n+\varrho)^2} + \frac{2\varrho^2}{\mathcal{C}} \leq \frac{\mathcal{M}\pi^2}{6} + \frac{2\varrho^2}{\mathcal{C}}.$$

Taking the expectation and employing $\mathbb{E} [\|v - \hat{v}^{(m)}\|^2] = \frac{\sigma^2}{m} = \mathbb{E} \left[\frac{z_m^2}{m} \right]$, we obtain

$$\tau_m^2 (k+1) \mathbb{E} [\|v - \hat{v}^{(m)}\|^2] \leq \frac{\mathcal{M}\pi^2}{6} + \frac{2\varrho^2}{\mathcal{C}} < \infty.$$

Letting $k \rightarrow \infty$, we get a contradiction. Hence \hat{k}_m must be finite. Finally from (38)

$$\frac{\mathcal{M}}{(\hat{k}_m + \varrho)^2} \leq \left(\frac{\tau_m}{\sqrt{m}} \right)^2 z_m^2 \rightarrow 0 \quad \text{as } m \rightarrow \infty.$$

Therefore, we must have $\hat{k}_m \rightarrow \infty$ as $m \rightarrow \infty$. Thus the result. \square

By virtue of Assumption 2.6, it directly follows that rule 1 determines a finite index k_m^* . If k_∞ is already finite, the statement is evident. Thus, we restrict our attention to the case $k_\infty = \infty$. According to rule 1, we have

$$\Omega(k, \hat{v}^{(m)}) = (k + \varrho) \|\mathcal{F}(u_k^{(m)}) - \hat{v}^{(m)}\|^2 \geq (k + \varrho) \kappa^2 \|v - \hat{v}^{(m)}\|^2.$$

Taking the expectation

$$(45) \quad \mathbb{E} [\Omega(k, \hat{v}^{(m)})] \geq (k + \varrho) \kappa^2 \mathbb{E} [\|v - \hat{v}^{(m)}\|^2] = (k + \varrho) \kappa^2 \mathbb{E} \left[\frac{z_m^2}{m} \right] \rightarrow \infty.$$

as $k \rightarrow \infty$. Hence, a finite integer k_m^* must exist at which $\Omega(k, \hat{v}^{(m)})$ attains its minimum. Building upon this observation, the next lemma establishes the main result of this subsection, and its proof is motivated by the approaches outlined in [49] and [45].

Lemma 4.3. *Suppose that $\mathcal{C} > 0$, as specified in (11), and that all the assumptions of Lemma 3.1 are satisfied. Let k_m^* denote the stopping index determined according to Rule 1. Then*

$$\Omega(k_m^*, \hat{v}^{(m)}) \rightarrow 0 \quad \text{as } m \rightarrow \infty.$$

Consequently,

$$\|\mathcal{F}(u_{k_m^*}^{(m)}) - \hat{v}^{(m)}\| \rightarrow 0 \quad \text{and} \quad k_m^* \mathbb{E} \left[\frac{z_m^2}{m} \right] \rightarrow 0 \quad \text{as } m \rightarrow \infty.$$

Proof. From (44) of the proof of Lemma 4.2, we have

$$\sum_{k=0}^{\hat{k}_m-1} \|\mathcal{F}(u_k^{(m)}) - \hat{v}^{(m)}\|^2 \leq \frac{2\varrho^2}{\mathcal{C}}.$$

By the minimality of $\Omega(k_m^*, \hat{v}^{(m)})$, we have

$$\|\mathcal{F}(u_k^{(m)}) - \hat{v}^{(m)}\|^2 = \frac{\Omega(k, \hat{v}^{(m)})}{k + \varrho} \geq \frac{\Omega(k_m^*, \hat{v}^{(m)})}{k + \varrho}.$$

Summing over $k = 0, 1, \dots, \hat{k}_m - 1$, it follows that

$$\sum_{k=0}^{\hat{k}_m-1} \frac{1}{k + \varrho} \Omega(k_m^*, \hat{v}^{(m)}) \leq \sum_{k=0}^{\hat{k}_m-1} \|\mathcal{F}(u_k^{(m)}) - \hat{v}^{(m)}\|^2 \leq \frac{2\varrho^2}{\mathcal{C}}.$$

Moreover,

$$\sum_{k=0}^{\hat{k}_m-1} \frac{1}{k+\varrho} \geq \int_0^{\hat{k}_m} \frac{dt}{t+\varrho} = \log\left(\frac{\hat{k}_m+\varrho}{\varrho}\right).$$

Hence,

$$\Omega(k_m^*, \hat{v}^{(m)}) \leq \frac{2\wp^2}{\mathcal{C} \log\left(\frac{\hat{k}_m+\varrho}{\varrho}\right)}.$$

Since $\hat{k}_m \rightarrow \infty$ as $m \rightarrow \infty$, we deduce that $\Omega(k_m^*, \hat{v}^{(m)}) \rightarrow 0$. The remaining assertions then follow directly from this convergence, together with Assumption 2.6 and (45). \square

4.2. Convergence. We now turn to the proof of the main result of this section. Prior to that, we establish a lemma that will play a key role in its derivation.

Lemma 4.4. *Suppose that $\mathcal{C} > 0$, as specified in (11), and that all the assumptions of Lemma 3.1 are satisfied. Let k_m^* denote the stopping index determined according to rule 1. Then $u_k^{(m)} \in \mathcal{B}_{3\wp}(u_0)$ for all $0 \leq k \leq k_m^*$ if m is sufficiently large.*

Proof. We proceed by induction. The claim is immediate for $k = 0$. Assume that $u_k^{(m)} \in \mathcal{B}_{3\wp}(u_0)$ for some $k < k_m^*$. Using (39), (40) and (41) we will show that $u_{k+1}^{(m)} \in \mathcal{B}_{3\wp}(u_0)$. By virtue of Young's inequality, it follows that for any $\mathcal{H} > 0$,

$$\|v - \hat{v}^{(m)}\| \|\mathcal{F}(u_k^{(m)}) - \hat{v}^{(m)}\| \leq \frac{1}{\mathcal{H}} \|\mathcal{F}(u_k^{(m)}) - \hat{v}^{(m)}\|^2 + \frac{\mathcal{H}}{4} \|v - \hat{v}^{(m)}\|^2.$$

Thus (40) becomes

$$(46) \quad \begin{aligned} -\langle g_k^{(m)}, h_k^{(m)} \rangle &\leq -(1-\eta)\alpha_k^{(m)} \|\mathcal{F}(u_k^{(m)}) - \hat{v}^{(m)}\|^2 + \wp\nu_0 \|\mathcal{F}(u_k^{(m)}) - \hat{v}^{(m)}\|^2 \\ &\quad + (1+\eta)\alpha_k^{(m)} \left(\frac{\mathcal{H}}{4} \|v - \hat{v}^{(m)}\|^2 + \frac{1}{\mathcal{H}} \|\mathcal{F}(u_k^{(m)}) - \hat{v}^{(m)}\|^2 \right). \end{aligned}$$

Combining (39), (46) and (41) we have

$$\begin{aligned} \|g_{k+1}^{(m)}\|^2 - \|g_k^{(m)}\|^2 &\leq \frac{(1+\eta)\zeta_1\mathcal{H}}{2} \|v - \hat{v}^{(m)}\|^2 \\ &\quad - 2 \left[\left(1 - \eta - \frac{1+\eta}{\mathcal{H}}\right) \zeta - \nu_0(\wp + \nu_1) - \zeta_0^2 \right] \|\mathcal{F}(u_k^{(m)}) - \hat{v}^{(m)}\|^2 \\ &\leq -2\mathcal{C} \|\mathcal{F}(u_k^{(m)}) - \hat{v}^{(m)}\|^2 + \mathcal{C}_1 \|v - \hat{v}^{(m)}\|^2 \end{aligned}$$

where $\mathcal{C}_1 = \frac{(1+\eta)\zeta_1\mathcal{H}}{2}$ and \mathcal{C} is the same positive constant as in (11). Therefore on Γ_m , we have

$$\begin{aligned} \|g_{k+1}^{(m)}\|^2 + 2\mathcal{C} \sum_{n=0}^k \|\mathcal{F}(u_n^{(m)}) - \hat{v}^{(m)}\|^2 &\leq \|g_0\|^2 + \mathcal{C}_1 \frac{(k+1)\tau_m^2 z_m^2}{\mathcal{H}^2 m} \\ &\leq \wp^2 + \left(\frac{\mathcal{C}_1 \tau_m^2}{\mathcal{H}^2} \right) \frac{k_m^* z_m^2}{m}. \end{aligned}$$

By Lemma 4.3 we can guarantee that $\left(\frac{\mathcal{C}_1 \tau_m^2}{\mathcal{H}^2}\right) \frac{k_m^* z_m^2}{m} \leq 3\wp^2$ for sufficiently large m . Thus, we have $\|u_{k+1}^{(m)} - u^\dagger\|^2 \leq 4\wp^2$. Since $\|u_0 - u^\dagger\| \leq \wp$, we therefore have $u_{k+1}^{(m)} \in \mathcal{B}_{3\wp}(u_0)$. \square

We are now in a position to present the main result of this section concerning Algorithm 2. The proof relies on the preceding lemma together with the stability result stated in Lemma 3.7 and Theorem 3.4.

Theorem 4.5. Suppose that $\mathcal{C} > 0$, as specified in (11), and that all the assumptions of Lemma 3.1 are satisfied. Let k_m^* denote the stopping index determined according to rule 1 for Algorithm 2, then a solution u^\dagger of (1) exists such that

$$\lim_{m \rightarrow \infty} \mathbb{E} \left[\|u_{k_m^*}^{(m)} - u^\dagger\|^2 \right] = 0.$$

Proof. Consider a sequence $\{m_r\}$ with $m_r \rightarrow \infty$ as $r \rightarrow \infty$, and let $\hat{v}^{(m_r)}$ denote the corresponding measurement data. For each pair $(m_r, \hat{v}^{(m_r)})$, let the stopping index defined by rule 1 be denoted by $k_r^* := k_{m_r}^*$.

Let u^\dagger represents the solution of (1) obtained in Theorem 3.4, satisfying $\|u_k - u^\dagger\| \rightarrow 0$ as $k \rightarrow \infty$, where $\{u_k\}_{k \geq 0}$ are the iterates generated by the exact-data version of Algorithm 2. To establish the desired result, we distinguish between two cases:

Case-I. Suppose that $k_r^* \rightarrow K$ for some finite integer $K > 0$ as $r \rightarrow \infty$. In this case, the proof proceeds in the same manner as the corresponding case in Theorem 3.8. Indeed, the argument requires only that

$$\|\mathcal{F}(u_K^{(m_r)}) - \hat{v}^{(m_r)}\| \rightarrow 0 \quad \text{as } r \rightarrow \infty,$$

which is guaranteed by Lemma 4.3.

Case-II. Suppose instead that $k_r^* \rightarrow \infty$. Then, for any fixed integer $k \geq 1$, we have $k_r^* > k$ for sufficiently large r . From the proof of Lemma 4.4, it follows that

$$\|u_{k+1}^{(m_r)} - u^\dagger\|^2 - \|u_k^{(m_r)} - u^\dagger\|^2 \leq \mathcal{C}_1 \|v - \hat{v}^{(m_r)}\|^2,$$

for all $0 \leq k < k_r^*$. Summing this inequality from k up to $k_r^* - 1$ yields

$$\|u_{k_r^*}^{(m_r)} - u^\dagger\|^2 \leq \|u_k^{(m_r)} - u^\dagger\|^2 + \mathcal{C}_1(k_r^* - k + 1) \|v - \hat{v}^{(m_r)}\|^2,$$

and, in particular,

$$\|u_{k_r^*}^{(m_r)} - u^\dagger\|^2 \leq \|u_k^{(m_r)} - u^\dagger\|^2 + \mathcal{C}_1 k_r^* \|v - \hat{v}^{(m_r)}\|^2.$$

The subsequent steps of the proof follows analogously to the similar case in the proof of Theorem 3.8. \square

5. NUMERICAL RESULTS AND PERFORMANCE ANALYSIS

This section details a series of numerical experiments designed to evaluate the effectiveness of the proposed algorithms, Algorithm 1 and Algorithm 2. Our analysis is particularly directed toward applications involving both linear and nonlinear ill-posed tomography problems. To implement the proposed method effectively, selecting appropriate initial reconstructors Ψ_θ is critical. In our experiments, we adopt three commonly used reconstruction methods: FBP, Tikhonov, and TV, whose detailed descriptions can be found in [5, Section 4.2]. The discrepancy principle and generalized cross-validation are used to choose the regularization parameters for the TV and Tikhonov methods, respectively. The Hann filter is employed to perform the FBP reconstruction.

To simulate realistic measurement conditions, independent and identically distributed (i.i.d.) Gaussian noise is added to the exact data v . Specifically, the i -th noisy measurement v_i is modeled as

$$v_i = v + \epsilon_i \frac{\xi}{\|\xi\|},$$

where ϵ_i denotes an independent Gaussian noise scalar, and ξ is a random vector drawn from the standard normal distribution.

The quantitative evaluation of the reconstructed images is performed using three standard image quality metrics: the relative error (RRE), the *Peak Signal-to-Noise Ratio (PSNR)*, and the *Structural Similarity Index (SSIM)* [47]. Since the pixel intensities are normalized within the range $[0, 1]$, the PSNR is defined as

$$\text{PSNR} := 20 \log_{10} \left(\frac{1}{\|u^\dagger - u_{k_m}^{(m)}\|} \right),$$

while the relative error is given by

$$\text{RRE} := \frac{\|u_{k_m}^{(m)} - u^\dagger\|}{\|u^\dagger\|},$$

where, $u_{k_m}^{(m)}$ denotes the reconstructed image obtained after k_m iterations of Algorithm 1, while u^\dagger represents the ground truth image. When employing Algorithm 2, we instead denote the reconstructed image by $u_{k_m^*}^{(m)}$ to reflect the use of the heuristic stopping criterion.

5.1. X-ray Computed Tomography. Computed Tomography (CT) is a vital medical imaging modality, used for diagnosing internal conditions like tumors, injuries, and fractures. The system operates by rotating an X-ray source around the subject, capturing the differential attenuation of beams across tissues via a detector array. The aggregated angular measurements constitute a sinogram. Mathematically, this process is modeled as a discretized linear system

$$(47) \quad \mathcal{F}_c u = \tilde{v},$$

where the matrix $\mathcal{F}_c \in \mathbb{R}^{m \times n}$ represents the discretized Radon transform, $u \in \mathbb{R}^n$ is the two-dimensional image vector (unknown), and $\tilde{v} \in \mathbb{R}^m$ is the measured, noisy sinogram. For a detailed treatment, see [43]. The vectorization of an $E \times F$ two-dimensional image, whose pixels are indexed by $a = (i, j)$, is performed lexicographically using either a row-major or column-major ordering. This process maps the image to a vector in \mathbb{R}^n , where $n = E \cdot F$.

In our tests, we incorporate the Operator Discretization Library (ODL) [1] to describe the image domain. Specifically, the function `odl.uniform_discr` is used to create a uniformly discretized $E \times F$ square grid over the region $[-128, 128]^2 \subset \mathbb{R}^2$. The Shepp–Logan phantom from `skimage.data` serves as the test image for the numerical simulations. The true image and the corresponding noisy sinograms, corrupted with Gaussian noise $\epsilon_i \sim \mathcal{N}(0, \varepsilon^2)$ where $\varepsilon = 10$, are presented in Fig. 2. Data acquisition simulates a parallel-beam CT geometry using `odl.tomo.parallel_beam_geometry` with $m_\theta = 60$ uniformly distributed projection angles over $[0, 2\pi)$. The forward operator \mathcal{F}_c is implemented via `odl.tomo.RayTransform`. For a 128×128 image ($n = 16,384$ pixels), ODL sets $d = \lceil \sqrt{2} \cdot 128 \rceil = 363$ detector elements, resulting in $m = 60 \cdot 363 = 21,780$ measurements. This overdetermined system ($m > n$) constitutes an ill-conditioned linear system. The parameters for (6) are empirically set to $R = 6$ and $\sigma = 0.05$. The step sizes α_k^δ and β_k^δ are chosen according to (9) and (10) with $\zeta_0 = 0.2$, $\zeta_1 = 0.5$, $\nu_0 = \nu_1 = 0.05$, and $\tau_m = 2m^{0.5}$. For rule 1, we select $\varrho = 100$.

First we generate the initial solution using FBP, Tik and TV. The initial solutions for the case $m = 10$ are shown in Fig. 3. Then we apply E-IRMGL+ Ψ (3) using both the stopping strategies and there reconstruction results are plotted in Fig. 4 and Fig. 5 for various cases of number of measurements m . A detailed comparison of the reconstruction quality and the corresponding number of iterations is provided in table 1. The results indicate that rule 2 performs better for a smaller number of measurement points (e.g., $m = 5$ and $m = 10$). However, as the number of measurements increases, the threshold value in rule 2 decreases, leading to a substantially larger number of iterations. In contrast, the stopping index determined by rule 1 is reached more quickly, owing to the oscillatory nature of the convergence behavior after several iterations. For the cases $m = 5$ and $m = 10$, the maximum number of iterations was set to 200, while for $m = 50$ and $m = 100$ it was increased to 500. These choices were guided by empirical observations and aimed

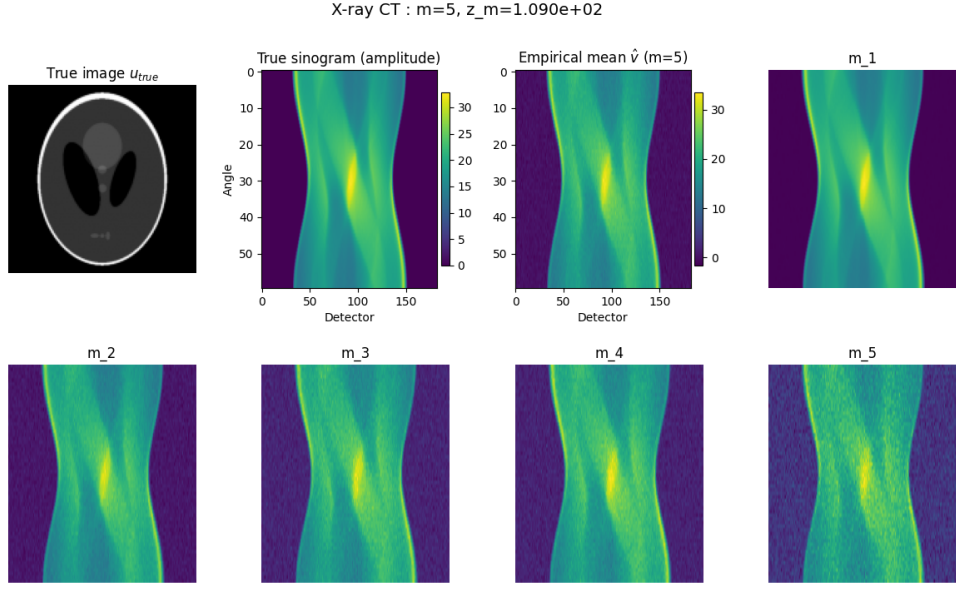


FIGURE 2. Exact solution for X-ray CT with 5 measured noisy sinograms and their empirical mean

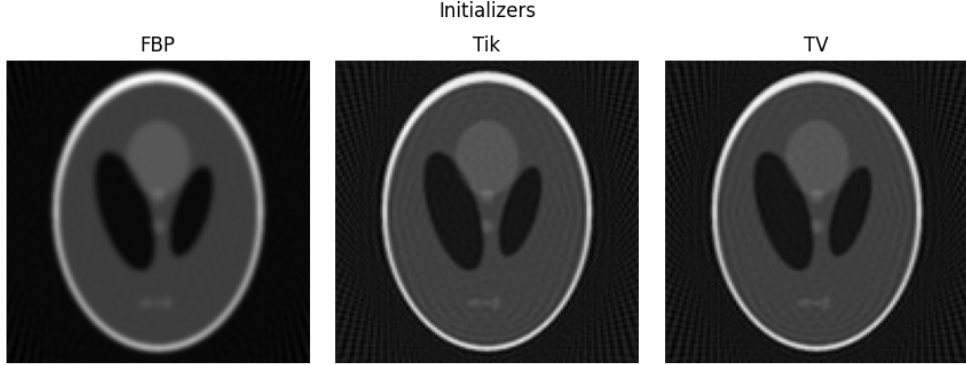
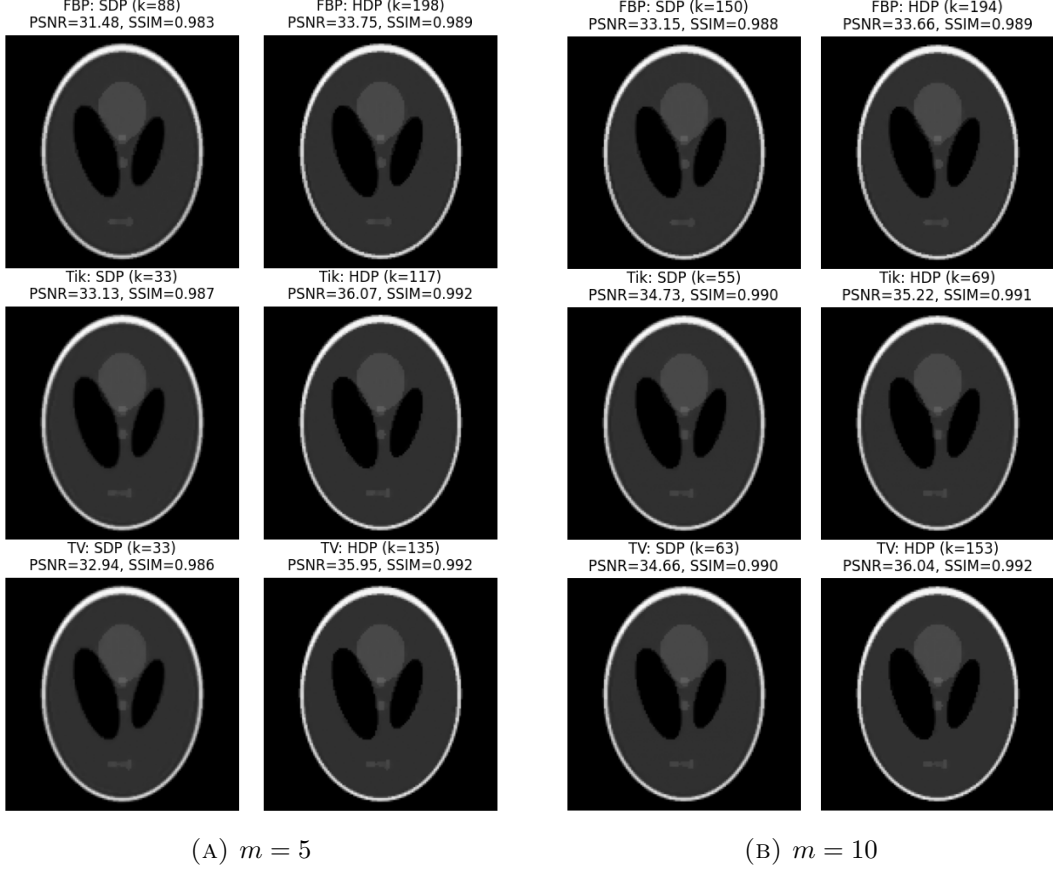


FIGURE 3. Reconstructed solutions of X-ray CT by using initializers with $m = 10$

at balancing computational efficiency with memory requirements. Other metrics like PSNR, SSIM and RRE are also plotted in Fig. 6, Fig. 7, Fig. 8 and Fig. 9 for each chosen value of m .

5.2. Phase retrieval CT. In this section, we consider the phase retrieval problem, which arises in numerous practical settings such as X-ray crystallography, microscopy, and related coherent imaging modalities, see [15] and the references therein. In conventional CT, detectors measure the attenuated X-ray intensity after logarithmic linearization, yielding a linear relation between the object and its projections, as described in (47). This model presumes that both amplitude and phase information of the measured signal are accessible. In contrast, in coherent imaging techniques such as X-ray phase-contrast tomography, propagation-based imaging, and coherent diffraction tomography, the detector records only the intensity (magnitude squared) of the transmitted or scattered wave field. Consequently, the reconstruction task becomes inherently nonlinear and is formulated as a phase retrieval inverse problem.

(A) $m = 5$ (B) $m = 10$ FIGURE 4. Reconstructed solutions of X-ray CT with $m = 5$ and $m = 10$

Mathematically, the phase retrieval problem in this context can be written as

$$(48) \quad \mathcal{F}_p(u) := |\mathcal{F}_c u|^2 = \tilde{v},$$

where $|\mathcal{F}_c u|^2$ denotes the element-wise squared magnitude of the projection data. Unlike the conventional linear CT model, this formulation is inherently nonlinear and nonconvex due to the loss of phase information. Consequently, the reconstruction of u from intensity-only measurements is significantly more challenging, as multiple solutions may correspond to the same magnitude data. To recover u , we employ Algorithm 1 and Algorithm 2. The proposed schemes are designed to handle the ill-posedness and nonlinearity of the phase retrieval problem.

Clearly \mathcal{F}_p is continuous differentiable and its Fréchet derivative $\mathcal{F}'_p(u) : \mathbb{R}^n \rightarrow \mathbb{R}^m$ is the linear map

$$\mathcal{F}'_p(u)[h] = 2(y \odot (\mathcal{F}_c h)) = 2(\text{diag}(y) \mathcal{F}_c)h,$$

where $h \in \mathbb{R}^n$, $y = \mathcal{F}_c u$ and \odot denotes the Hadamard (element wise) product. Thus, the Jacobian matrix is given by

$$J(u) = \mathcal{F}'_p(u) = 2 \text{ diag}(\mathcal{F}_c u) \mathcal{F}_c \in \mathbb{R}^{m \times n}.$$

The adjoint of the derivative $\mathcal{F}'_p(u)$ is the map $\mathcal{F}'_p(u)^* : \mathbb{R}^m \rightarrow \mathbb{R}^n$, given by

$$\mathcal{F}'_p(u)^*[w] = 2 \mathcal{F}_c^\top ((\mathcal{F}_c u) \odot w), \quad \text{for any } w \in \mathbb{R}^m.$$

Equivalently, in matrix form,

$$(49) \quad \mathcal{F}'_p(u)^* = 2 \mathcal{F}_c^\top \text{ diag}(\mathcal{F}_c u).$$

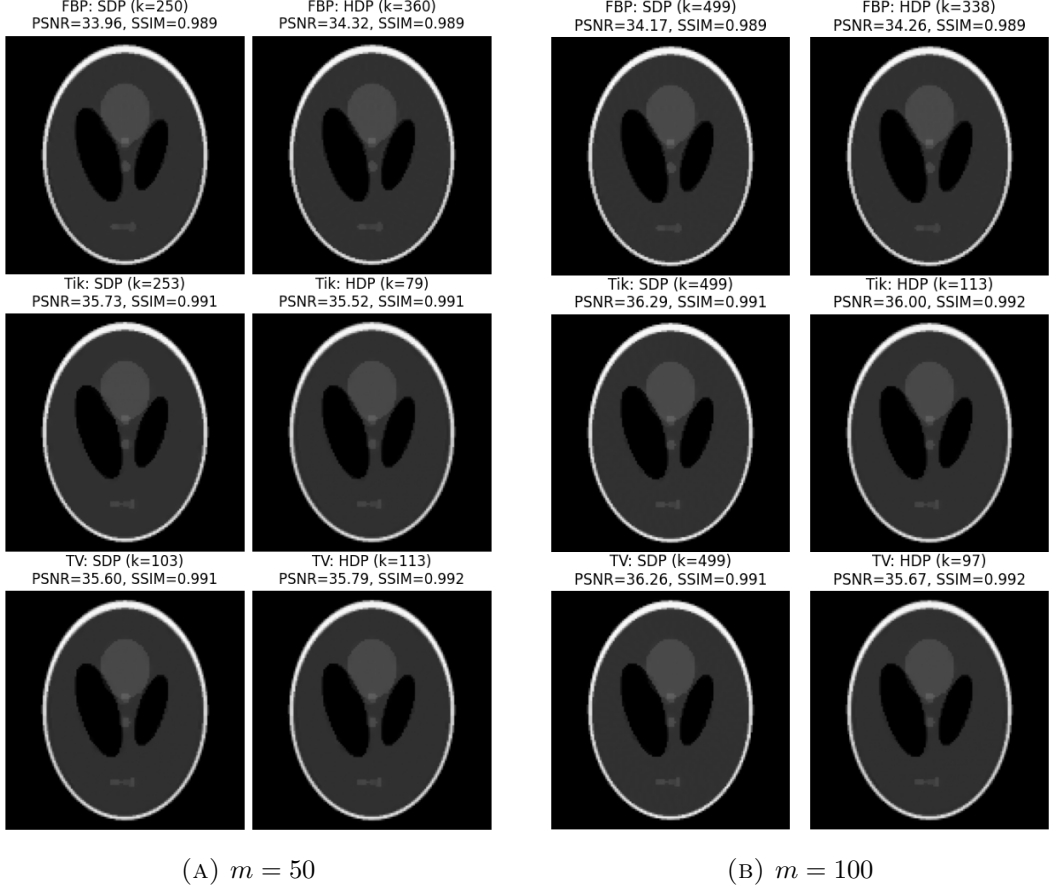


FIGURE 5. Reconstructed solutions of X-ray CT with $m = 50$ and $m = 100$

We use (48) and (49) to apply E-IRMGL+ Ψ method. The numerical simulations are conducted using the `binary_blobs` available in the `skimage.data` library. The ground truth image and the corresponding noisy sinograms, contaminated with Gaussian noise $\epsilon_i \sim \mathcal{N}(0, \epsilon^2)$ with $\epsilon = 10$, are illustrated in Fig. 10. We set $\tau_m = 3m^{0.5}$ for rule 2, while for rule 1, the parameter ϱ is chosen as 1000 and the maximum number of iteration is chosen to be 300. Algorithm 1 and Algorithm 2 are initialized using FBP, Tikhonov, and TV methods, with the results for $m = 10$ displayed in Fig. 11. Subsequently, the E-IRMGL+ Ψ scheme (3) is applied with both stopping strategies, and the corresponding reconstructions for different measurement numbers m are shown in Fig. 12. In table 2, we summarizes the performance comparison of the two stopping strategies in the context of the phase retrieval problem.

6. CONCLUDING REMARKS

This study introduces and analyzes a novel graph-based iterative regularization method for solving nonlinear ill-posed inverse problems. The proposed method is examined under two distinct stopping criteria, namely the statistical discrepancy principle and the heuristic discrepancy principle. Unlike conventional approaches, the framework does not require the knowledge of the noise level. Instead, it employs the mean of i.i.d. estimators to approximate it. Comprehensive analyses of stability, regularity, and convergence are carried out under both stopping rules, based on standard local assumptions on the forward operator \mathcal{F} and general conditions on initializers Ψ_θ . The theoretical findings are further supported and validated through detailed numerical experiments

TABLE 1. Numerical comparison of both algorithms for X-ray CT by using different values of m .

m	Ψ	Algorithm 1				Algorithm 2			
		Iter.	RRE	PSNR	SSIM	Iter.	RRE	PSNR	SSIM
5	FBP	88	0.114	31.48	0.9831	198	0.088	33.75	0.9889
	Tik	33	0.099	33.13	0.9865	117	0.067	36.07	0.9916
	TV	33	0.097	32.94	0.9863	135	0.068	35.95	0.9917
10	FBP	150	0.094	33.15	0.9879	194	0.089	33.66	0.9888
	Tik	55	0.078	34.73	0.9900	69	0.074	35.22	0.9908
	TV	63	0.079	34.66	0.9901	153	0.068	36.04	0.9915
50	FBP	250	0.086	33.96	0.9891	360	34.32	0.9893	0.082
	Tik	253	0.071	35.73	0.9908	79	0.071	35.52	0.9912
	TV	103	0.071	35.60	0.9914	113	35.79	0.9916	0.069
100	FBP	max	0.084	34.17	0.9888	338	0.083	34.26	0.9892
	Tik	max	0.066	36.29	0.9914	113	0.068	36.00	0.9917
	TV	max	0.066	36.26	0.9911	97	0.070	35.67	0.9916

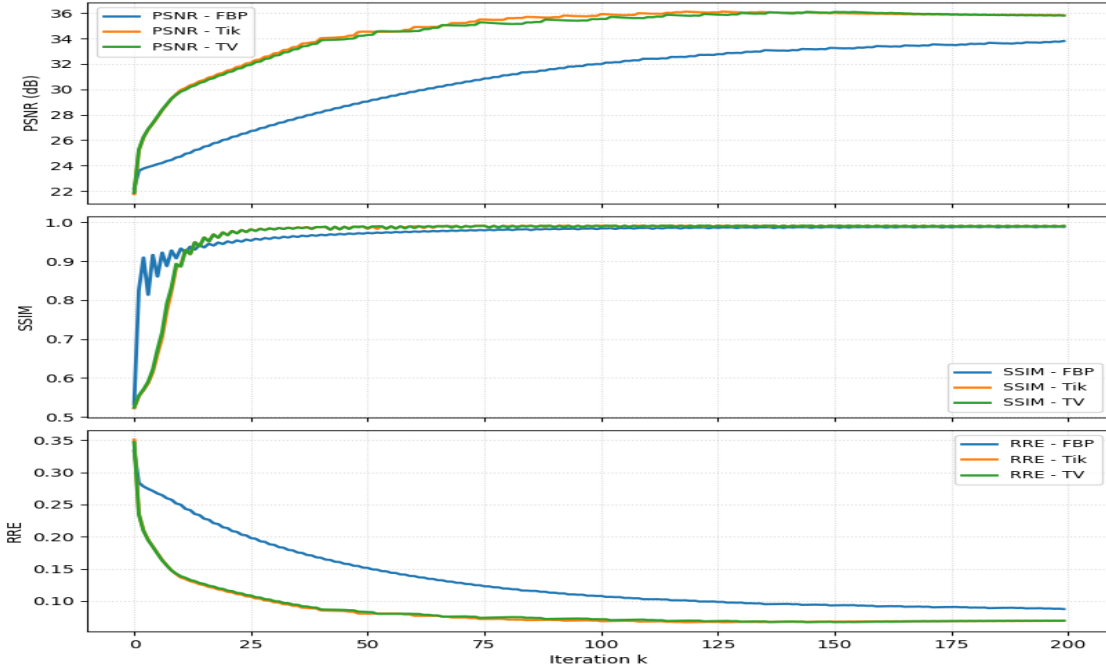
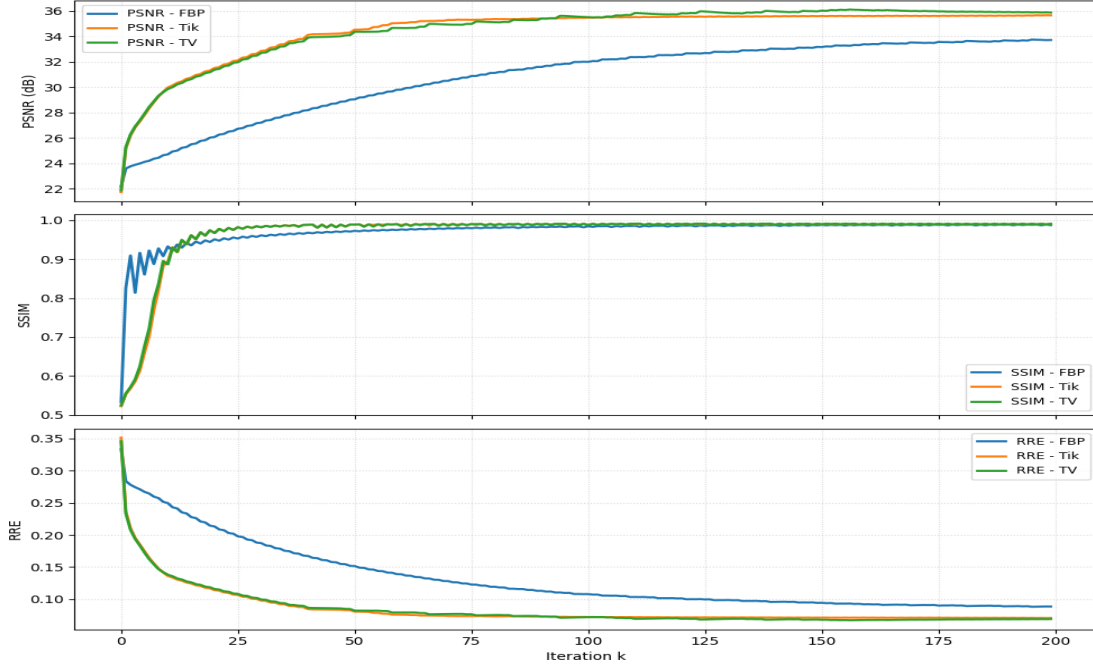
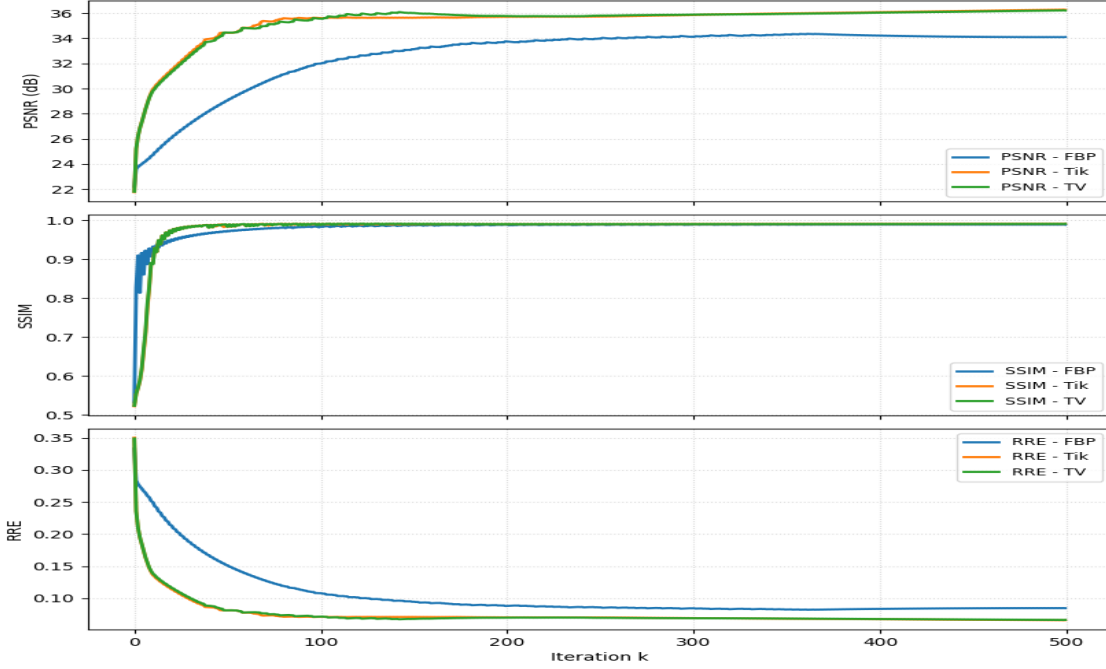


FIGURE 6. PSNR, SSIM and RRE curves of X-ray CT for $m = 5$

and comparative studies on two numerical examples, including X-ray CT and phase retrieval CT problems.

The proposed framework has been developed within a finite-dimensional setting. As a potential direction for future research, it would be of significant interest to extend the convergence analysis to infinite-dimensional Hilbert or Banach space frameworks.

FIGURE 7. PSNR, SSIM and RRE curves of X-ray CT for $m = 10$ FIGURE 8. PSNR, SSIM and RRE curves of X-ray CT for $m = 50$

DATA AVAILABILITY

On reasonable request, the authors will provide the datasets and source code created during this study.

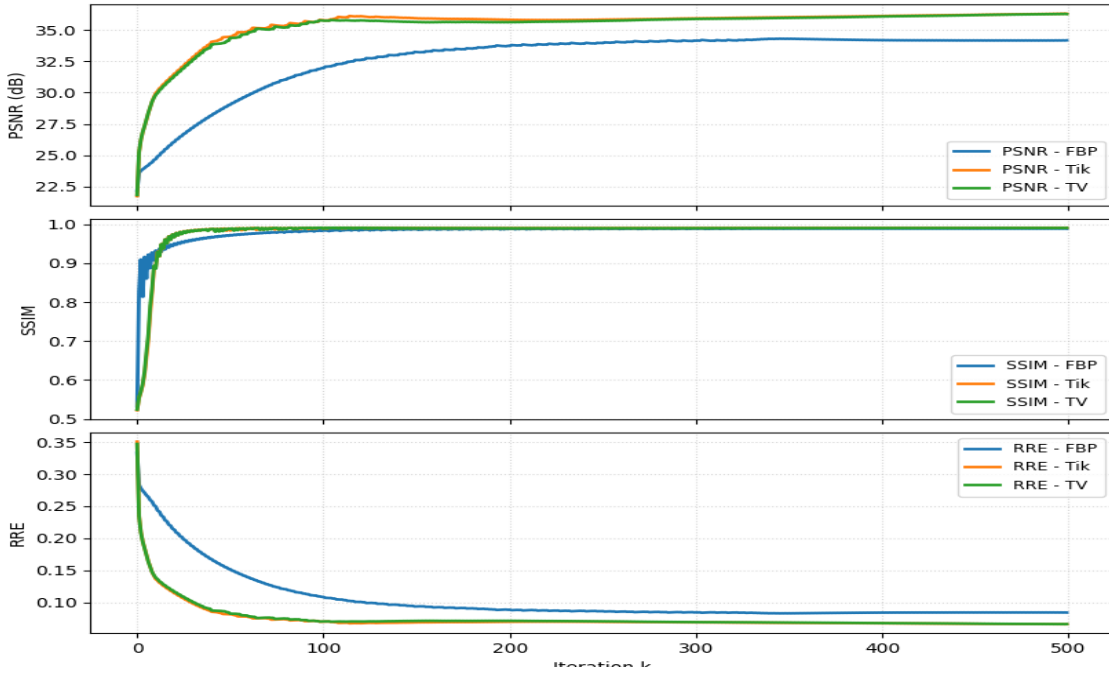
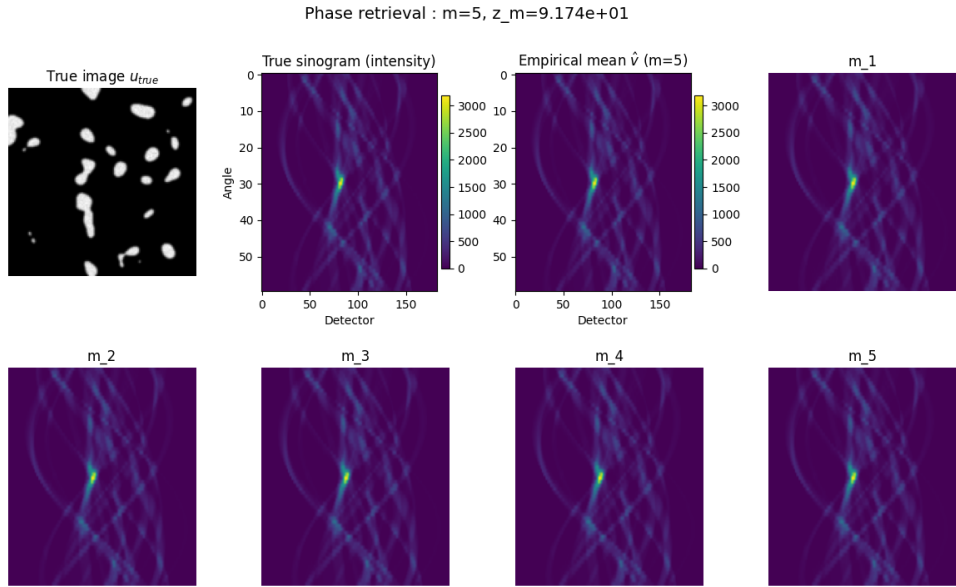
FIGURE 9. PSNR, SSIM and RRE curves of X-ray CT for $m = 100$ 

FIGURE 10. Exact solution for phase retrieval CT with 5 measured sinograms and their empirical mean

REFERENCES

[1] J. Adler, H. Kohr, A. Ringh, J. Moosmann, sbanert, M. J. Ehrhardt, G. R. Lee, niinimaki, bgris, O. Verdier, J. Karlsson, zickert, W. J. Palenstijn, O. Öktem, C. Chen, H. A. Loarca, and M. Lohmann. odlgroup/odl: Odl 0.7.0, sep 2018.

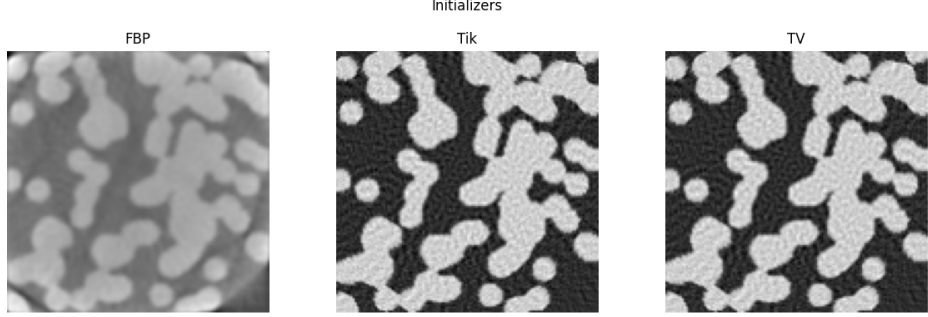


FIGURE 11. Reconstructed solutions of phase retrieval CT by using initializers with $m = 10$

TABLE 2. Numerical comparison of both algorithms for phase retrieval CT by using different values of m .

m	Ψ	Algorithm 1				Algorithm 2			
		Iter.	RRE	PSNR	SSIM	Iter.	RRE	PSNR	SSIM
5	FBP	150	0.155	19.21	0.7669	292	0.235	20.40	0.7947
	Tik	98	0.145	19.79	0.7636	274	0.124	21.08	0.8008
	TV	97	0.147	19.67	0.7605	277	0.125	21.07	0.8017
10	FBP	198	0.143	19.88	0.7786	286	0.133	20.54	0.7900
	Tik	152	0.135	20.43	0.7777	280	0.122	21.23	0.7947
	TV	134	0.136	20.43	0.7771	295	0.122	21.27	0.7970

- [2] A. Aspri, S. Banert, O. Öktem, and O. Scherzer. A data-driven iteratively regularized landweber iteration. *Numerical Functional Analysis and Optimization*, 41(10):1190–1227, 2020.
- [3] A. Aspri, Y. Korolev, and O. Scherzer. Data driven regularization by projection. *Inverse Problems*, 36(12):125009, 2020.
- [4] H. Bajpai, G. Mittal, and A. K. Giri. Hanke-raus heuristic rule for iteratively regularized stochastic gradient descent. *arXiv preprint arXiv:2412.02397*, 2024.
- [5] H. Bajpai, G. Mittal, and A. K. Giri. On the convergence of iterative regularization method assisted by the graph laplacian with early stopping. *SIAM Journal on Imaging Sciences*, 2025. Accepted for publication.
- [6] H. Bajpai, G. Mittal, and A. K. Giri. Stochastic data-driven bouligand–landweber method for solving non-smooth inverse problems. *Journal of Inverse and Ill-posed Problems*, 33(2):153–170, 2025.
- [7] A. B. Bakushinskii. Remarks on choosing a regularization parameter using the quasioptimality and ratio criterion. *USSR Computational Mathematics and Mathematical Physics*, 24(4):181–182, 1985.
- [8] H. H. Barrett. Image reconstruction and the solution of inverse problems in medical imaging. In *Medical Images: Formation, Handling and Evaluation*, pages 3–42. Springer, 1992.
- [9] D. Bianchi, F. Bossmann, W. Wang, and M. Liu. Improved impedance inversion by deep learning and iterated graph laplacian. *arXiv preprint arXiv:2404.16324*, 2024.
- [10] D. Bianchi, D. Evangelista, S. Aleotti, M. Donatelli, E. L. Piccolomini, and W. Li. A data-dependent regularization method based on the graph laplacian. *SIAM Journal on Scientific Computing*, 47(2):C369–C398, 2025.
- [11] L. Bottou, F. E. Curtis, and J. Nocedal. Optimization methods for large-scale machine learning. *SIAM review*, 60(2):223–311, 2018.
- [12] M. M. Bronstein, J. Bruna, Y. LeCun, A. Szlam, and P. Vandergheynst. Geometric deep learning: going beyond euclidean data. *IEEE Signal Processing Magazine*, 34(4):18–42, 2017.
- [13] L. Calatroni, Y. van Gennip, C.-B. Schönlieb, H. M. Rowland, and A. Flenner. Graph clustering, variational image segmentation methods and hough transform scale detection for object measurement in images. *Journal of Mathematical Imaging and Vision*, 57:269–291, 2017.

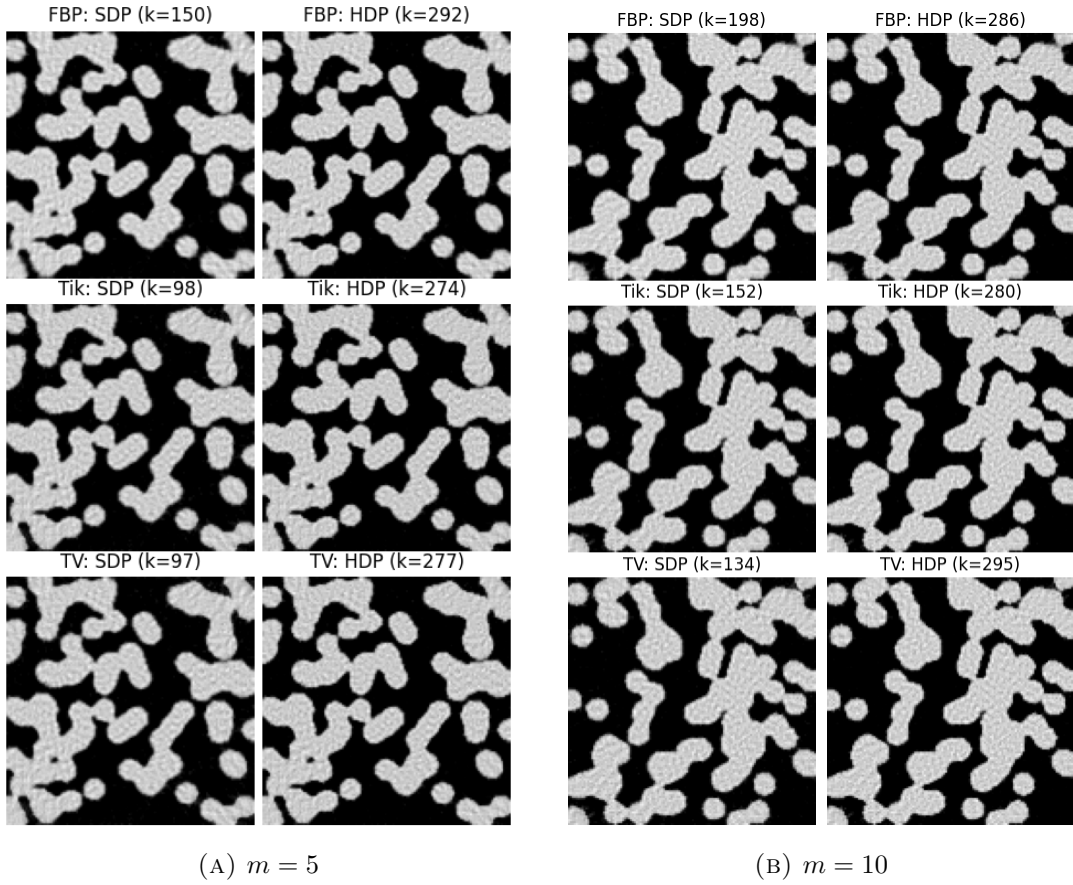
(A) $m = 5$ (B) $m = 10$

FIGURE 12. Reconstructed solutions of phase retrieval CT with $m = 50$ and $m = 100$

- [14] H. W. Engl, M. Hanke, and A. Neubauer. *Regularization of inverse problems*, volume 375. Springer Science & Business Media, 1996.
- [15] A. Fannjiang and T. Strohmer. The numerics of phase retrieval. *Acta Numerica*, 29:125–228, 2020.
- [16] Z. Fu, Q. Jin, Z. Zhang, B. Han, and Y. Chen. Analysis of a heuristic rule for the irgnm in banach spaces with convex regularization terms. *Inverse problems*, 36(7):075002, 2020.
- [17] Z. Fu, W. Wang, B. Han, and Y. Chen. Two-point landweber-type method with convex penalty terms for nonsmooth nonlinear inverse problems. *IMA Journal of Numerical Analysis*, 43(2):1115–1148, 2023.
- [18] G. Gilboa and S. Osher. Nonlocal operators with applications to image processing. *Multiscale Modeling & Simulation*, 7(3):1005–1028, 2009.
- [19] M. Hanke, A. Neubauer, and O. Scherzer. A convergence analysis of the landweber iteration for nonlinear ill-posed problems. *Numerische Mathematik*, 72(1):21–37, 1995.
- [20] M. Hanke and T. Raus. A general heuristic for choosing the regularization parameter in ill-posed problems. *SIAM Journal on Scientific Computing*, 17(4):956–972, 1996.
- [21] B. Harrach, T. Jahn, and R. Potthast. Beyond the bakushinkii veto: regularising linear inverse problems without knowing the noise distribution. *Numerische Mathematik*, 145(3):581–603, 2020.
- [22] B. Harrach, T. Jahn, and R. Potthast. Regularizing linear inverse problems under unknown non-gaussian white noise allowing repeated measurements. *IMA Journal of Numerical Analysis*, 43(1):443–500, 2023.
- [23] U. Hassan and M. S. Anwar. Reducing noise by repetition: introduction to signal averaging. *European Journal of Physics*, 31(3):453, 2010.
- [24] S. Hubmer, E. Sherina, S. Kindermann, and K. Raik. A numerical comparison of some heuristic stopping rules for nonlinear landweber iteration. In *ETNA-Electronic Transactions on Numerical Analysis*, pages 216–241. Österreichische Akademie der Wissenschaften (ÖAW), 2022.

- [25] B. Jadamba, A. Khan, and M. Sama. Inverse problems of parameter identification in partial differential equations. In *Mathematics In Science And Technology: Mathematical Methods, Models and Algorithms in Science and Technology*, pages 228–258. World Scientific, 2011.
- [26] T. Jahn. A modified discrepancy principle to attain optimal convergence rates under unknown noise. *Inverse problems*, 37(9):095008, 2021.
- [27] B. Jin and D. A. Lorenz. Heuristic parameter-choice rules for convex variational regularization based on error estimates. *SIAM Journal on Numerical Analysis*, 48(3):1208–1229, 2010.
- [28] Q. Jin. Hanke-raus heuristic rule for variational regularization in banach spaces. *Inverse Problems*, 32(8):085008, 2016.
- [29] Q. Jin. On a heuristic stopping rule for the regularization of inverse problems by the augmented lagrangian method. *Numerische Mathematik*, 136(4):973–992, 2017.
- [30] Q. Jin. Convergence rates of landweber-type methods for inverse problems in banach spaces. *Inverse Problems*, 41(4):045011, 2025.
- [31] Q. Jin and W. Wang. Dual gradient method for ill-posed problems using multiple repeated measurement data. *Inverse Problems*, 39(8):085005, 2023.
- [32] Q. Jin and M. Zhong. On the iteratively regularized gauss–newton method in banach spaces with applications to parameter identification problems. *Numerische Mathematik*, 124(4):647–683, 2013.
- [33] A. C. Kak and M. Slaney. *Principles of computerized tomographic imaging*. SIAM, 2001.
- [34] B. Kaltenbacher, A. Neubauer, and O. Scherzer. *Iterative regularization methods for nonlinear ill-posed problems*. Walter de Gruyter, 2008.
- [35] P. Kearey, M. Brooks, and I. Hill. *An introduction to geophysical exploration*. John Wiley & Sons, 2013.
- [36] M. Keller, D. Lenz, and R. K. Wojciechowski. *Graphs and discrete Dirichlet spaces*, volume 358. Springer, 2021.
- [37] S. Kindermann and K. Raik. Convergence of heuristic parameter choice rules for convex tikhonov regularization. *SIAM Journal on Numerical Analysis*, 58(3):1773–1800, 2020.
- [38] H. Liu, R. Real, X. Lu, X. Jia, and Q. Jin. Heuristic discrepancy principle for variational regularization of inverse problems. *Inverse Problems*, 36(7):075013, 2020.
- [39] Y. Lou, X. Zhang, S. Osher, and A. Bertozzi. Image recovery via nonlocal operators. *Journal of Scientific Computing*, 42(2):185–197, 2010.
- [40] R. G. Lyons. *Understanding digital signal processing*, 3/E. Pearson Education India, 1997.
- [41] G. Mittal, H. Bajpai, and A. K. Giri. Convergence analysis of iteratively regularized landweber iteration with uniformly convex constraints in banach spaces. *Journal of Complexity*, 86:101897, 2025.
- [42] V. Morozov. On the solution of functional equations by the method of regularization. *Doklady Akademii Nauk SSSR*, 167(3):510, 1966.
- [43] F. Natterer. *The mathematics of computerized tomography*. SIAM, 2001.
- [44] A. Neubauer. On landweber iteration for nonlinear ill-posed problems in hilbert scales. *Numerische Mathematik*, 85(2):309–328, 2000.
- [45] R. R. Real. Hanke–raus rule for landweber iteration in banach spaces. *Numerische Mathematik*, 156(1):345–373, 2024.
- [46] O. Scherzer, M. Grasmair, H. Grossauer, M. Haltmeier, and F. Lenzen. *Variational methods in imaging*, volume 167. Springer, 2009.
- [47] Z. Wang, A. C. Bovik, H. R. Sheikh, and E. P. Simoncelli. Image quality assessment: from error visibility to structural similarity. *IEEE transactions on image processing*, 13(4):600–612, 2004.
- [48] N. Yu, Y. Xia, Z. Fu, and Y. Chen. Landweber–kaczmarz method for inverse problems using multiple repeated measurements. *Inverse Problems and Imaging*, pages 0–0, 2025.
- [49] Z. Zhang and Q. Jin. Heuristic rule for non-stationary iterated tikhonov regularization in banach spaces. *Inverse Problems*, 34(11):115002, 2018.
- [50] Z. Zhou. On the convergence of a data-driven regularized stochastic gradient descent for nonlinear ill-posed problems. *SIAM Journal on Imaging Sciences*, 18(1):388–448, 2025.